

Spin-Adapted Fermionic Unitaries: From Lie Algebras to Compact Quantum Circuits

I. Magoulas* and F.A. Evangelista

*Department of Chemistry and Cherry Emerson Center for Scientific Computation,
Emory University, Atlanta, Georgia 30322, USA*

Conservation of symmetries plays a crucial role in both classical and quantum simulations of many-body systems, enabling the tracking of states with specific symmetry properties and leading to substantial reductions in the number of optimization parameters. The design of efficient quantum circuits that enforce all symmetries typically encountered in chemistry has remained elusive, mainly due to the interplay of point group and spin symmetries. By exploiting Lie algebraic techniques, we derive exact product formulas representing symmetry-adapted unitaries. These decompositions allow us to design the most efficient symmetry-preserving quantum circuits to date. Finally, we introduce a minimum universal symmetry-adapted operator pool to further reduce the required quantum resources.

Keywords: fermionic algebra, quantum many-body theory, quantum computing, spin-adaptation

I. INTRODUCTION

The simulation of quantum many-body systems, such as those encountered in chemistry, condensed matter physics, and materials science, has long been identified as a killer application for quantum computers [1–4]. In the non-relativistic regime, the correlated motion of particles comprising such systems is governed by the Schrödinger equation. Although the computational resources required to solve the Schrödinger equation exactly in a finite basis grow combinatorially with system size [5], an ideal quantum device would require, in principle, a number of qubits that scales only linearly [2, 6–9]. Beyond academic interest, pushing the boundaries of system sizes amenable to computational treatment, both in the numbers of particles and basis functions, will have a transformative effect in many fields, including, for example, catalysis, photochemistry, energy-storage materials, biology, and strongly correlated systems [10–12]. However, access to a fault-tolerant quantum computer capable of rapid, noise-free simulations of large quantum systems would be of no practical value if the results were unreliable or outright wrong.

A major barrier hindering the practical utility of quantum simulations is the proper enforcement of the symmetries characterizing the system of interest. In the context of chemical applications, for example, the electronic Hamiltonian conserves the number of particles N , the projection of the total spin on the z axis S_z , the total spin squared S^2 , and the irreducible representation of the molecular point group. Arguably, the most important aspect of symmetry adaptation is the disentangling of states with different symmetry properties. Indeed, if a quantum algorithm violates even one of the inherent symmetries of the problem of interest, there is always a risk of collapsing into a state with undesired symme-

try. This issue is particularly problematic because error-mitigation techniques [13], such as postselection [14], are generally ineffective in this scenario. To be precise, although postselection based on the targeted symmetry eigenvalue is useful in restoring symmetries artificially broken due to device noise [15, 16], it cannot be applied when the state produced by the noiseless quantum algorithm belongs to a wrong symmetry sector. These observations emphasize the need for quantum algorithms that rigorously respect all available symmetries. Moreover, respecting symmetries in quantum simulations offers several advantages [17]. To begin with, the dimension of the many-electron Hilbert space is significantly reduced when symmetry constraints are enforced, resulting in far fewer optimization parameters to obtain accurate or even numerically exact results. Furthermore, for adaptive algorithms [18–20], symmetry adaptation leads to smaller operator pools and, hence, fewer measurements during the operator selection process.

In this work, we employ Lie-algebraic techniques to design compact quantum circuits that rigorously enforce all the symmetries of the electronic Hamiltonian relevant to chemical systems. Specifically, we use the Wei–Norman decomposition [21, 22] to express symmetry-adapted unitaries exactly as a product of elementary, spinorbital unitaries. The individual components respect the particle-number, S_z , and spatial symmetries by construction, while the exactness of the decomposition ensures that their product enforces S^2 symmetry as well. Furthermore, we construct efficient circuit representations of the individual unitaries that enable their hardware implementation. Finally, we introduce a minimum, universal symmetry-adapted operator pool to further reduce the resources required for quantum simulations.

* ilias.magoulas@emory.edu

II. SYMMETRY ENFORCEMENT IN QUANTUM SIMULATIONS

One can classify techniques to enforce symmetries into three categories: 1) a broad set of approaches that do not require substantial algorithmic or state-preparation modifications, 2) techniques to produce a symmetry-adapted initial state, and 3) symmetry-preserving quantum gates. Within the first category, one approach is symmetry restoration via projection [23, 24]. Although, as already mentioned, projection after variation, *i.e.*, postselection, is not ideal, variation after projection is more robust and resource-efficient because the optimization occurs in the symmetry-adapted Hilbert space. This technique is general and can be used to restore any symmetries of interest, including spatial (*e.g.*, point-group) [25, 26], spin [26–30], and particle-number [30–32] symmetries. Nevertheless, symmetry projectors are typically implemented as linear combinations of unitaries (LCU) [33, 34], which introduce ancilla registers and many controlled operations, inflating the controlled-NOT (CNOT) count.

An alternative strategy is the incorporation of penalty terms in the Hamiltonian that artificially raise the energy of states with undesired symmetries [35–38] (see, also, [39]). In doing so, the quantum simulations are biased toward states with desired symmetry properties. Although such approaches are general, they typically require a large number of measurements, depend on user-defined hyperparameters, and the optimization is formally occurring on the full, rather than symmetry-adapted, Hilbert space.

In qubit reduction techniques [40–42], one takes advantage of \mathbb{Z}_2 symmetries of the Hamiltonian, including number parities and point group symmetry, to block diagonalize the Hamiltonian and eliminate redundant qubits. The quantum simulation is subsequently performed on the Hamiltonian block with the targeted \mathbb{Z}_2 symmetries. Although these schemes reduce the required quantum resources, in their current formulation they are not applicable to more generic symmetries, such as S^2 .

In the second family of methods, a few strategies have been proposed for the preparation of spin eigenfunctions on quantum devices [43–46]. In [43, 44, 46], a single configuration state function is realized on the quantum device, serving as a good initial guess for algorithms such as quantum phase estimation [47]. However, the approximate implementation of the time-evolution operator can still introduce symmetry contaminants. The symmetry-preserving preparation circuits of [45] construct a hyper-spherical parametrization of the exact ground state and, thus, are impractical. Alternatively, one can transform the computational basis states from encoding Slater determinants to representing configuration state functions via the quantum Schur transform [48]. The issue with this approach is that it requires a register of qudits whose count and local dimension depend on the system size. This difficulty can be circumvented by employing a truncated spin-adapted basis [49], albeit introducing an approximation.

Methods in the third category employ unitaries that preserve symmetries by construction. In general, a unitary operator can be expressed either as $\exp(-iH)$ with a Hermitian generator H , as in time evolution and quantum phase estimation [47], or as $\exp(A)$ with an anti-Hermitian generator A , which is typical in ansatz construction. Of these two forms, the latter has received considerable attention, because electronic-structure simulations are a key target for current noisy and near-fault-tolerant quantum hardware. Notable examples in this family of methods are the quantum-number-preserving (QNP) gate fabric [50], the discretely optimized variational quantum eigensolver (DISCO-VQE) [51], and the tiled unitary product states (tUPS) approach [52]. These schemes rely on essentially the same set of elementary, symmetry-preserving unitaries, namely, the singlet spin-adapted singles and perfect pairing doubles operator pool. They rigorously enforce the particle-number, S_z , and S^2 symmetries, but need to violate spatial symmetry to attain universality. As a result, quantum simulations based on these techniques may variationally collapse to states with undesired symmetry.

III. GENERATORS OF SYMMETRY-ADAPTED FERMIONIC UNITARIES

Arguably the most natural approach to locally enforce the key symmetries relevant to molecular quantum simulations is to employ operator pools relying on fermionic excitation operators, typically based on the unitary extension [53–65] of coupled-cluster theory [66–71]. The most widely used pool in this category consists of anti-Hermitian fermionic generalized single,

$$A_p^q = a_q^\dagger a_p - a_p^\dagger a_q, \quad (1)$$

and double,

$$A_{pq}^{rs} = a_r^\dagger a_s^\dagger a_q a_p - a_p^\dagger a_q^\dagger a_s a_r, \quad (2)$$

excitation operators [72, 73], commonly denoted as GSD. Here, indices p , q , r , and s denote generic spinorbitals, and a_p (a_p^\dagger) is the annihilation (creation) operator associated with the p -th spinorbital. The popularity of the GSD pool can be attributed to the following advantages. Although composed of low-rank many-body operators, it is universal if each operator can appear multiple times in the ansatz with independent optimization parameters [74]. The construction of efficient quantum circuit implementations of GSD unitaries is enabled through the fermionic excitation-based (FEB) formulation [75, 76]. Finally, GSD operators satisfy particle-number symmetry by construction, while the enforcement of S_z and point-group symmetries is straightforward by imposing appropriate restrictions on the excitation indices [17].

A persistent limitation of the GSD operator pool is the enforcement of S^2 symmetry, which requires the replacement of Eqs. (1) and (2) by their singlet spin-adapted

counterparts [77–84]. Using the notation in which P , Q , R , and S index generic spatial orbitals, and the $s_z = -\frac{1}{2}$ and $s_z = \frac{1}{2}$ spin functions are designated as \downarrow and \uparrow , respectively, the singlet spin-adapted singles take the form

$$\begin{aligned} A_P^Q &= \frac{1}{\sqrt{2}} \left(A_{P\uparrow}^{Q\uparrow} + A_{P\downarrow}^{Q\downarrow} \right) \\ &= \frac{1}{\sqrt{2}} \left(a_{Q\uparrow}^\dagger a_{P\uparrow} + a_{Q\downarrow}^\dagger a_{P\downarrow} - \text{h.c.} \right). \end{aligned} \quad (3)$$

The corresponding double excitations can be grouped into four distinct cases:

$$\begin{aligned} A_{PP}^{QQ} &= A_{P\uparrow P\downarrow}^{Q\uparrow Q\downarrow} \\ &= a_{Q\uparrow}^\dagger a_{Q\downarrow}^\dagger a_{P\downarrow} a_{P\uparrow} - \text{h.c.}, \end{aligned} \quad (4)$$

$$A_{PP}^{QR} = \frac{1}{\sqrt{2}} \left(A_{P\uparrow P\downarrow}^{Q\uparrow R\downarrow} - A_{P\uparrow P\downarrow}^{Q\downarrow R\uparrow} \right), \quad (5)$$

$${}^{[0]}A_{PQ}^{RS} = \frac{1}{2} \left(A_{P\uparrow Q\downarrow}^{R\uparrow S\downarrow} - A_{P\uparrow Q\downarrow}^{R\downarrow S\uparrow} - A_{P\downarrow Q\uparrow}^{R\uparrow S\downarrow} + A_{P\downarrow Q\uparrow}^{R\downarrow S\uparrow} \right), \quad (6)$$

and

$$\begin{aligned} {}^{[1]}A_{PQ}^{RS} &= \frac{1}{\sqrt{3}} \left[A_{P\uparrow Q\uparrow}^{R\uparrow S\uparrow} + A_{P\downarrow Q\downarrow}^{R\downarrow S\downarrow} \right. \\ &\quad \left. + \frac{1}{2} \left(A_{P\uparrow Q\downarrow}^{R\uparrow S\downarrow} + A_{P\uparrow Q\downarrow}^{R\downarrow S\uparrow} + A_{P\downarrow Q\uparrow}^{R\uparrow S\downarrow} + A_{P\downarrow Q\uparrow}^{R\downarrow S\uparrow} \right) \right], \end{aligned} \quad (7)$$

with the “[0]” and “[1]” superscripts in Eqs. (6) and (7) denoting the common intermediate spin quantum number characterizing the PQ and RS orbital pairs. The singlet spin-adapted GSD pool is comprised of the operators in Eqs. (3) to (7) and is typically denoted as saGSD. The design of efficient quantum circuits representing unitaries generated by singlet spin-adapted operators is straightforward in the case of single [Eq. (3)] and perfect-pairing double [Eq. (4)] excitations, which define the operator pool typically denoted as saGSpD [50–52]. The issue with designing efficient quantum circuits for unitaries generated by the more complicated singlet spin-adapted double excitation operators [Eqs. (5) to (7)] lies in the fact that naïve product formulas based on, for example, Trotterization or the Zassenhaus identity, violate spin symmetry.

IV. SYMMETRY-ADAPTED CIRCUITS: LINEAR COMBINATION OF UNITARIES

We have recently shown that spin-adapted unitaries can be exactly represented as a finite series [17] (see also [85]), enabling their circuit implementation via the LCU approach [33, 34]. For example, the unitary generated by

A_{PP}^{QR} is exactly expressed as [17]

$$\begin{aligned} e^{\theta A_{PP}^{QR}} &= I \\ &+ \left\{ \sin \left(\frac{\theta}{\sqrt{2}} \right) + \frac{1}{\sqrt{2}} \left[\sin(\theta) - \sqrt{2} \sin \left(\frac{\theta}{\sqrt{2}} \right) \right] \right. \\ &\quad \times (h_{Q\downarrow R\uparrow} + n_{Q\downarrow R\uparrow}) (h_{Q\uparrow R\downarrow} + n_{Q\uparrow R\downarrow}) \left(A_{P\uparrow P\downarrow}^{Q\uparrow R\downarrow} - A_{P\uparrow P\downarrow}^{Q\downarrow R\uparrow} \right) \\ &+ \sin^2 \left(\frac{\theta}{2} \right) (h_{P\uparrow P\downarrow} + n_{P\uparrow P\downarrow}) \left(A_{Q\uparrow R\downarrow}^{Q\downarrow R\uparrow} + A_{Q\downarrow R\uparrow}^{Q\uparrow R\downarrow} \right) \\ &+ \left[\cos \left(\frac{\theta}{\sqrt{2}} \right) - 1 \right] [(h_{Q\uparrow R\downarrow} + h_{Q\downarrow R\uparrow}) n_{P\uparrow P\downarrow} \\ &\quad + (n_{Q\uparrow R\downarrow} + n_{Q\downarrow R\uparrow}) h_{P\uparrow P\downarrow}] \\ &+ \left[\cos(\theta) - 2 \cos \left(\frac{\theta}{\sqrt{2}} \right) + 1 \right] (h_{P\uparrow P\downarrow} n_{Q\uparrow R\downarrow} h_{R\uparrow R\downarrow} \\ &\quad + h_{Q\uparrow Q\downarrow R\uparrow R\downarrow} n_{P\uparrow P\downarrow}) \\ &+ \frac{1}{2} \left[\cos(\theta) - 2 \cos \left(\frac{\theta}{\sqrt{2}} \right) + 1 \right] (h_{P\uparrow P\downarrow} n_{Q\uparrow R\downarrow} n_{Q\downarrow R\uparrow} \\ &\quad + h_{P\uparrow P\downarrow} n_{Q\downarrow R\uparrow} n_{P\uparrow P\downarrow} + h_{Q\downarrow R\uparrow} n_{P\uparrow P\downarrow} n_{Q\uparrow R\downarrow} \\ &\quad + h_{Q\uparrow R\downarrow} n_{P\uparrow P\downarrow} n_{Q\downarrow R\uparrow}), \end{aligned} \quad (8)$$

with θ being a real parameter, and n and h denoting collections of particle ($n_p = a_p^\dagger a_p$, $n_{pq\dots} = n_p n_q \dots$) and hole ($h_p = a_p a_p^\dagger$, $h_{pq\dots} = h_p h_q \dots$) number operators, respectively. By translating Eq. (8) to the qubit space using the fermionic encoding of choice, *e.g.*, Jordan–Wigner [86] or Bravyi–Kitaev [87] mappings, the spin-adapted unitary is expressed as a linear combination of Pauli strings with θ -dependent coefficients,

$$e^{\theta A_{PP}^{QR}} = \sum_{i=0}^{M-1} c_i(\theta) P_i. \quad (9)$$

Since Pauli strings are Hermitian involutions, they are unitary, rendering Eq. (9) an LCU.

The LCU circuit implementation of spin-adapted unitaries is shown in Fig. 1. In addition to the number of qubits needed to realize the trial state $|\Psi\rangle$ on which the spin-adapted unitary will act, the circuit requires $\lceil \log_2(M) \rceil$ ancillas, with M being the number of terms in the LCU [Eq. (9)]. Besides the PREPARE gate and its adjoint acting on the ancillas, the circuit applies the Pauli strings to $|\Psi\rangle$, controlled by the ancilla qubits. To understand the mechanism with which the LCU circuit realizes $\exp(\theta A) |\Psi\rangle$, with A being a spin-adapted operator [Eqs. (5) to (7)], we examine the state of the quantum

computer $|QC\rangle$ at the time-slices shown in Fig. 1:

$$\begin{aligned}
|QC\rangle &\xrightarrow{\text{step 1}} |0\rangle^{\otimes \lceil \log_2(M) \rceil} \otimes |\Psi\rangle \\
&\xrightarrow{\text{step 2}} \sum_{i=0}^{M-1} \sqrt{\frac{c_i(\theta)}{\|\mathbf{c}(\theta)\|_1}} |i\rangle \otimes |\Psi\rangle \\
&\xrightarrow{\text{step 3}} \sum_{i=0}^{M-1} \sqrt{\frac{c_i(\theta)}{\|\mathbf{c}(\theta)\|_1}} |i\rangle \otimes P_i |\Psi\rangle \\
&\xrightarrow{\text{step 4}} \frac{1}{\|\mathbf{c}(\theta)\|_1} |0\rangle^{\otimes \lceil \log_2(M) \rceil} \otimes \sum_{i=0}^{M-1} c_i(\theta) P_i |\Psi\rangle + \dots \\
&= \frac{1}{\|\mathbf{c}(\theta)\|_1} |0\rangle^{\otimes \lceil \log_2(M) \rceil} \otimes e^{\theta A} |\Psi\rangle + \dots,
\end{aligned} \tag{10}$$

with

$$\|\mathbf{c}(\theta)\|_1 \equiv \sum_{i=0}^{M-1} c_i(\theta). \tag{11}$$

(Note that in writing Eq. (10), any signs have been incorporated in the Pauli strings, leaving the $c_i(\theta)$ coefficients strictly positive.) Therefore, if the measurement outcome on the ancilla register is the all-zero state, the quantum circuit in Fig. 1 has applied the spin-adapted unitary to the trial state $|\Psi\rangle$. The probability of obtaining this outcome is the inverse square of the 1-norm of the LCU coefficients.

The advantage of the quantum circuit of Fig. 1 is that it implements an exact representation of the spin-adapted unitary, rigorously enforcing all desired symmetries. Furthermore, the number of terms M in the LCU is independent of the identity of the excitation indices, depending only on the type of generator (A_{PP}^{QR} vs. ${}^{[0]}A_{PQ}^{RS}$ vs. ${}^{[1]}A_{PQ}^{RS}$) and on the chosen fermionic encoding. Unfortunately, the LCU approach has its own complications. To begin with, the number of terms M is quite large, even when one considers unitaries generated by the simpler singlet spin-adapted double excitation operator A_{PP}^{QR} . This, in turn, implies that the number of ancilla qubits and multiqubit-controlled Pauli gates will be very large. The hardware implementation of the PREPARE gate will introduce additional multiqubit-controlled gates, although their number and nature depends on the form of the $c_i(\theta)$ coefficients. Furthermore, as described above, the success probability of postselecting the ancillas in the all-zero state is $1/\|\mathbf{c}(\theta)\|_1^2$. Oblivious amplitude amplification can improve the success rate to near-deterministic [34, 88, 89], while postselection can be completely bypassed by viewing the LCU as a block-encoding [90] of the spin-adapted unitary and taking advantage of the qubitization algorithm [91, 92]. However, even with these approaches, the tremendous burden on the quantum resources remains. To make matters worse, the circuit of Fig. 1 implements a single spin-adapted unitary, while typical ansätze are expressed as a product of

many such operators. All the above render the LCU approach unattractive for implementing spin-adapted unitaries, even in a fault-tolerant setting.

V. SYMMETRY-ADAPTED CIRCUITS: WEI–NORMAN DECOMPOSITION

To address these difficulties, we introduce exact decompositions of unitaries generated by singlet spin-adapted double excitation operators into products of spinorbital unitaries. This is accomplished via the Lie-algebraic technique known as the Wei–Norman decomposition [21, 22]. In brief, this approach allows us to express $\exp(\theta A)$, a rotation generated by $A = \sum_i c_i A_i$, as an ordered product $\prod_i \exp(\alpha_i(\theta) E_i)$, where $\{E_i\}$ is a fixed ordered basis for the dynamical Lie algebra \mathfrak{g} obtained from the Lie closure of $\{A_i\}$, and the θ -dependent coefficients $\alpha_i(\theta)$ are determined by the Wei–Norman equations. From a bird’s-eye view, the Wei–Norman decomposition algorithm proceeds as follows [93, 94]:

1. Select the target unitary, $U(\theta) \equiv \exp(\theta \sum_i c_i A_i)$.
2. Select an ordered basis $\{E_i\}$ of the dynamical Lie algebra $\mathfrak{g} \equiv \text{Lie}(\{A_i\})$ and express the generator A of the target unitary in this basis:

$$A = \sum_i d_i E_i. \tag{12}$$

3. Use θ -dependent parameters $\{\alpha_i(\theta)\}$ to postulate the factorization

$$e^{\theta \sum_i d_i E_i} = \prod_i e^{\alpha_i(\theta) E_i}, \tag{13}$$

with initial conditions $\alpha_i(0) = 0$.

4. Differentiate Eq. (13) with respect to θ to obtain

$$\sum_i d_i E_i U(\theta) = \sum_i \alpha'_i(\theta) (\bar{E}_i)_{i-1\dots 1} U(\theta), \tag{14}$$

where $\alpha'_i(\theta) = \frac{d\alpha_i(\theta)}{d\theta}$ and, omitting the θ -dependence of the α_i parameters for clarity,

$$\begin{aligned}
(\bar{E}_i)_{i-1\dots 1} &= e^{\alpha_1 E_1} \dots e^{\alpha_{i-1} E_{i-1}} E_i e^{-\alpha_{i-1} E_{i-1}} \dots e^{-\alpha_1 E_1} \\
&= \sum_j M_{ji}(\alpha_1, \dots, \alpha_{i-1}) E_j
\end{aligned} \tag{15}$$

5. Left-multiply Eq. (14) by $U^{-1}(\theta)$ and equate the coefficients of the basis elements $\{E_i\}$ on both sides of the equality to obtain the Wei–Norman system of coupled ordinary differential equations for $\{\alpha_i(\theta)\}$, which can be expressed in matrix form as

$$\begin{aligned}
\mathbf{M}(\alpha_1, \alpha_2, \dots)(\alpha'_1, \alpha'_2, \dots)^\top &= (d_1, d_2, \dots)^\top \Rightarrow \\
(\alpha'_1, \alpha'_2, \dots)^\top &= \mathbf{M}^{-1}(\alpha_1, \alpha_2, \dots)(d_1, d_2, \dots)^\top
\end{aligned} \tag{16}$$

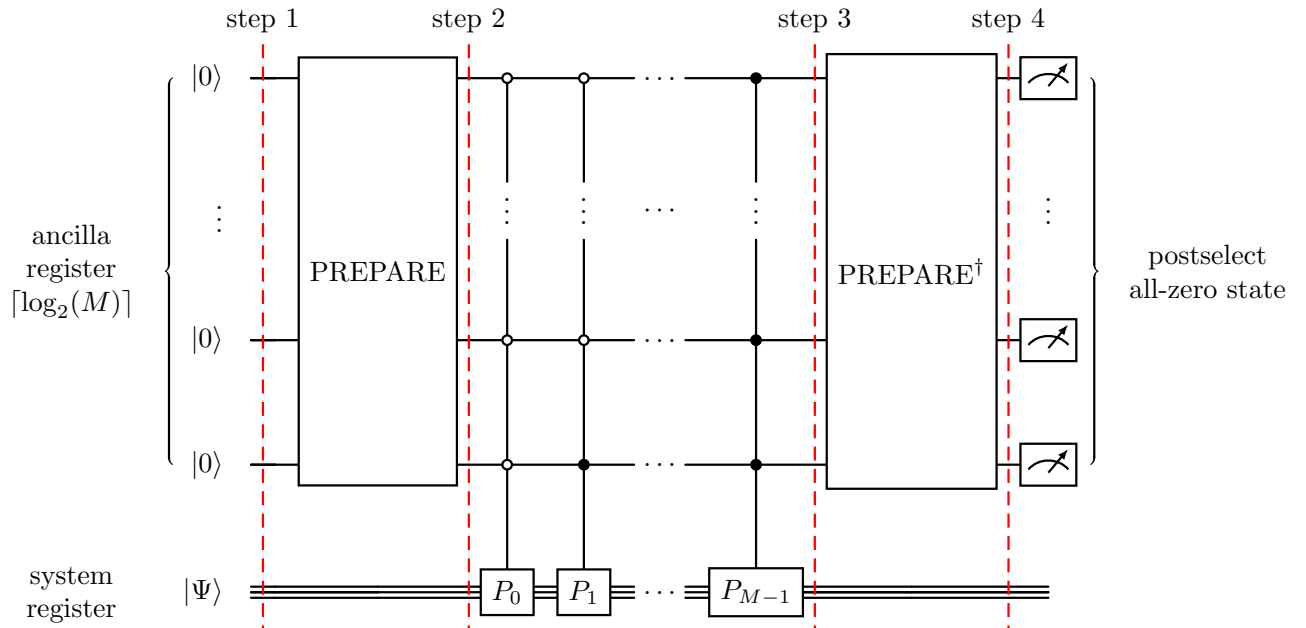


FIG. 1. Quantum circuit implementation of unitary generated by a singlet spin-adapted double excitation operator. The system register is initialized in the state on which the spin-adapted unitary will act. Open and full circles denote controls based on the $|0\rangle$ and $|1\rangle$ states, respectively. The gates P_0 through P_{M-1} represent the Pauli strings appearing in the LCU decomposition of the spin-adapted unitary.

6. Solve Eq. (16) in the nonsingular $\det(\mathbf{M}) \neq 0$ region of interest to obtain the numerical values of the θ -dependent parameters $\alpha_i(\theta)$.

There are two degrees of freedom that affect the Wei–Norman decomposition. The first is the choice of basis of the dynamical Lie algebra, and the second is the ordering of the exponentials in the product formula. By appropriately choosing these degrees of freedom, one may obtain Wei–Norman systems that are nonsingular on the region of interest, easier to solve, or even admit closed-form solutions.

The practical utility of the Wei–Norman decomposition for expressing symmetry-adapted unitaries faces two main challenges. The first concerns the availability of analytic expressions for the unitary transformations in Eq. (15). The second concerns the existence of efficient quantum-circuit implementations for the elementary unitaries appearing in the final product formula. To address the first challenge, we employ the exact, closed-form expressions for fermionic unitary transformations that we recently derived [95]. To address the second, we rely on the fermionic excitation-based (FEB) formalism, originally developed for generalized single and double excitations by Yordanov *et al.* [75] and extended to arbitrary-rank excitations by us [96].

As an illustration of the Wei–Norman decomposition, we focus on the simplest, yet non-trivial, spin-adapted unitary generated by A_{PP}^{QR} [Eq. (5)]. In the first step, we compute the Lie closure of $\{A_{P\uparrow P\downarrow}^{Q\uparrow R\downarrow}, A_{P\uparrow P\downarrow}^{Q\downarrow R\uparrow}\}$, and obtain that the dynamical Lie algebra \mathfrak{g} is spanned by

$$\mathfrak{g} = \text{span} \left\{ \begin{array}{l} A_{P\uparrow P\downarrow}^{Q\uparrow R\downarrow}, \\ A_{P\uparrow P\downarrow}^{Q\downarrow R\uparrow}, \\ A_{P\uparrow P\downarrow}^{Q\uparrow R\uparrow}, \\ A_{P\uparrow P\downarrow}^{Q\downarrow R\uparrow} (h_{Q\downarrow R\uparrow} + n_{Q\downarrow R\uparrow}), \\ A_{P\uparrow P\downarrow}^{Q\uparrow R\uparrow} (h_{Q\uparrow R\downarrow} + n_{Q\uparrow R\downarrow}), \\ A_{Q\uparrow R\downarrow}^{Q\downarrow R\uparrow} (h_{P\uparrow P\downarrow} - n_{P\uparrow P\downarrow}) \end{array} \right\}, \quad (17)$$

$$\equiv \{E_1, E_2, E_3, E_4, E_5\}$$

where, for the sake of brevity, we denote the basis elements as $\{E_i\}_{i=1}^5$. As shown in Section SIII of the Supplemental Material, this 5-dimensional Lie algebra is isomorphic to the Lie algebra direct sum $\mathbb{R}^2 \oplus \mathfrak{so}(3) \cong \mathbb{R}^2 \oplus \mathfrak{su}(2)$. As far as the many-body nature of the basis elements is concerned, E_1 and E_2 are the spinorbital excitation operators defining the singlet spin-adapted generator A_{PP}^{QR} . The remaining elements E_3 – E_5 are four-body operators, each containing a two-body anti-Hermitian excitation component multiplied by a linear combination of two particle-hole-conjugate number operator strings [see Eq. (17) and Tables SI and SII in the Supplemental Material]. Despite this complication, in Section SII of the Supplemental Material we demonstrate that these types of generators satisfy $E_j^3 = -E_j$ and $E_j[E_i, E_j]E_j = 0$. These are the necessary and sufficient conditions for the unitary transformation to be exactly expressed as [95]

In the next step, we postulate the factorization of the spin-adapted unitary as

$$e^{\frac{\theta}{\sqrt{2}}(E_1 - E_2)} = \prod_{i=1}^5 e^{\alpha_i E_i}, \quad (18)$$

with α_i being θ -dependent parameters. Note that, in our notation, products with ascending indices are ordered from left to right and conversely for descending indices. To determine the values of the parameters, we differentiate Eq. (18) with respect to θ and work as follows to obtain [94]:

$$\begin{aligned} & \frac{1}{\sqrt{2}} (E_1 - E_2) e^{\frac{\theta}{\sqrt{2}}(E_1 - E_2)} \\ &= \sum_{i=1}^5 \alpha'_i \prod_{j=1}^{i-1} e^{\alpha_j E_j} E_i \prod_{k=i}^5 e^{\alpha_k E_k} \\ &= \sum_{i=1}^5 \alpha'_i \prod_{j=1}^{i-1} e^{\alpha_j E_j} E_i \prod_{k=i-1}^1 e^{-\alpha_k E_k} \prod_{l=1}^5 e^{\alpha_l E_l} \\ &= \sum_{i=1}^5 \alpha'_i (\bar{E}_i)_{i-1 \dots 1} e^{\theta \frac{1}{\sqrt{2}}(E_1 - E_2)}, \end{aligned} \quad (19)$$

where in the last step we used Eq. (18), and the similarity transformations are defined as

$$(\bar{E}_2)_1 \equiv e^{\alpha_1 E_1} E_2 e^{-\alpha_1 E_1}, \quad (20a)$$

$$(\bar{E}_3)_{21} \equiv e^{\alpha_1 E_1} e^{\alpha_2 E_2} E_3 e^{-\alpha_2 E_2} e^{-\alpha_1 E_1}, \dots \quad (20b)$$

In principle, unitary transformations of fermionic operators cannot be expressed in a closed form, as they give rise to a non-terminating Hausdorff expansion. Nevertheless, we have recently shown that in special cases the commutator expansion can be re-summed to a closed form involving only the single and doubly nested commutators multiplied by trigonometric functions [95]. The unitary transformations required for the Wei–Norman decompositions of spin-adapted unitaries involve more complicated fermionic operators than those we considered before, containing an anti-Hermitian component multiplied, at most, by a linear combination of two particle-hole-conjugate number-operator strings [see Eq. (17) and Tables SI and SII in the Supplemental Material]. Despite this complication, in Section SII of the Supplemental Material we demonstrate that these types of generators satisfy $E_j^3 = -E_j$ and $E_j[E_i, E_j]E_j = 0$. These are the necessary and sufficient conditions for the unitary transformation to be exactly expressed as [95]

$$\begin{aligned} e^{\alpha_j E_j} E_i e^{-\alpha_j E_j} &= E_i - \sin(\alpha_j) [E_i, E_j] \\ &+ [1 - \cos(\alpha_j)] [[E_i, E_j], E_j]. \end{aligned} \quad (21)$$

Using Eq. (21), we compute all pertinent similarity transformations appearing in Eq. (19). By equating the coefficients of the generators E_i appearing on both sides of Eq. (19), we arrive at a system of coupled ordinary

differential equations for the θ -dependent parameters α_i . The first two differential equations are trivial, namely,

$$\alpha'_1 = \frac{1}{\sqrt{2}} \quad (22)$$

and

$$\alpha'_2 = -\frac{1}{\sqrt{2}}, \quad (23)$$

and, using the initial conditions $\alpha_i = 0$, can be readily integrated to give $\alpha_1(\theta) = \frac{\theta}{\sqrt{2}}$ and $\alpha_2(\theta) = -\frac{\theta}{\sqrt{2}}$. Using these relations, the remaining differential equations, expressed in matrix form, read

$$\mathbf{M} \begin{pmatrix} \alpha'_3 \\ \alpha'_4 \\ \alpha'_5 \end{pmatrix} = \begin{pmatrix} 0 \\ \frac{\cos\left(\frac{\theta}{\sqrt{2}}\right) - 1}{\sqrt{2}} \\ \frac{\sin\left(\frac{\theta}{\sqrt{2}}\right)}{\sqrt{2}} \end{pmatrix} \quad (24)$$

with the Wei–Norman coefficient matrix \mathbf{M} given by

$$\mathbf{M} = \begin{pmatrix} c_\theta & -s_\theta s_3 & c_\theta s_4 - s_\theta c_3 c_4 \\ -s_\theta^2 & c_\theta c_3 - c_\theta s_\theta s_3 & -s_\theta^2 s_4 - c_\theta s_3 c_4 - c_\theta s_\theta c_3 c_4 \\ c_\theta s_\theta & s_\theta c_3 + c_\theta^2 s_3 & c_\theta^2 c_3 c_4 + c_\theta s_\theta s_4 - s_\theta s_3 c_4 \end{pmatrix}, \quad (25)$$

where we define $c_\theta \equiv \cos\left(\frac{\theta}{\sqrt{2}}\right)$, $s_\theta \equiv \sin\left(\frac{\theta}{\sqrt{2}}\right)$, $c_i \equiv \cos(\alpha_i)$, and $s_i \equiv \sin(\alpha_i)$. It can be shown that $\det(\mathbf{M}) = \cos(\alpha_4)$, and thus the Wei–Norman decomposition of Eq. (18) is exact everywhere except at the singularities $\theta = (2\kappa + 1)\frac{\pi}{2}$, $\kappa \in \mathbb{Z}$. Solving the above system of ordinary differential equations analytically is at least impractical, if not impossible. To that end, we employed SciPy [97] to integrate it numerically (see Section SI of the Supplemental Material for the computational details).

The results of the numerical integration in the $\theta \in [0, 10]$ region, including the α_1 and α_2 parameters, are given in Fig. 2. It is interesting to note that the first two factors in the Wei–Norman decomposition of $\exp(A_{PP}^{QR})$ are equivalent to its first-order Trotterization, a consequence of the structure of the dynamical Lie algebra [see Eq. (17) and Section SIII of the Supplemental Material]. The remaining three factors provide the required correction to render the final decomposition exact. We have recently shown [17] that, in contrast to unitaries generated by spinorbital operators which are periodic functions of the angle θ , spin-adapted unitaries are almost periodic [98]. As can be seen in Fig. 2, the almost-periodicity of the Wei–Norman decomposition of Eq. (18) can be attributed to the last three exponentials, whose parameters seem to oscillate with incommensurate periods. In the first panel in Fig. S1 in the Supplemental Material, we provide the results of the numerical integration in the region $\theta \in [-100, 100]$, which extends well-beyond the physical range of amplitudes encountered in typical chemistry applications. In this panel, we note that

$|\alpha_4(\theta)| < \frac{\pi}{2}$, $\theta \in [-100, 100]$, rendering the decomposition Eq. (18) exact for the entire range of θ values considered in this work.

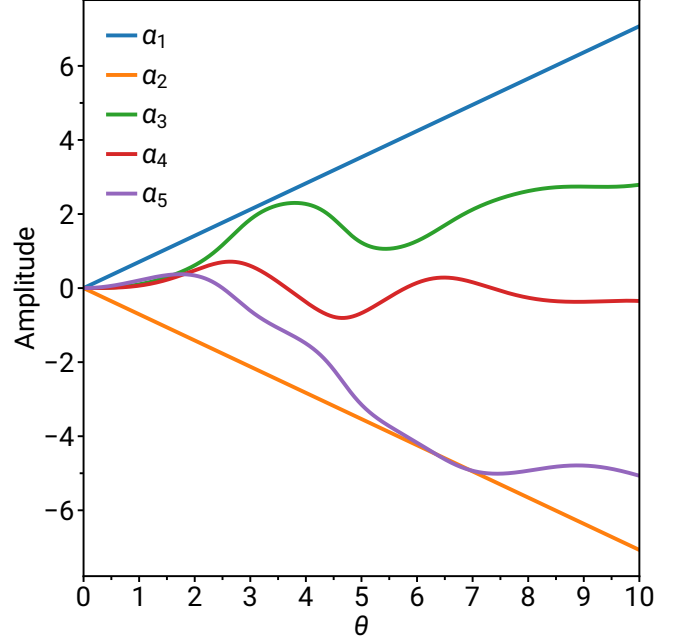


FIG. 2. Numerical values of the θ -dependent parameters defining the Wei–Norman decomposition of $\exp(\theta A_{PP}^{QR})$ [Eq. (18)].

At this point, it is worth commenting on the aforementioned two degrees of freedom affecting the Wei–Norman decomposition. Since the dynamical Lie algebras characterizing the examined spin-adapted unitaries are not abelian, different orderings of exponentials in the product formula will lead to different systems of coupled differential equations. For the simpler case of A_{PP}^{QR} , we examined all 120 permutations of the five basis elements of the associated dynamical Lie algebra [Eq. (17)]. In Figs. S1–S5 in the Supplemental Material, for each permutation, we show the results of the numerical integration in the extended region $\theta \in [-100, 100]$. A quick inspection of these figures reveals that α_1 – α_4 are odd functions of θ , while α_5 is even. Furthermore, for more than one third of the permutations we encountered singularities, limiting the numerical integration to a small region. As anticipated from the structure of the underlying dynamical Lie algebra, the angles of the unitaries generated by $A_{P\uparrow P\downarrow}^{Q\uparrow R\downarrow}$ and $A_{P\uparrow P\downarrow}^{Q\downarrow R\uparrow}$ matched their counterparts from the first-order Trotterization of A_{PP}^{QR} . However, the remaining three parameters were quite sensitive to the ordering of the exponentials. Nevertheless, the parameters were always varying more or less slowly with the angle θ , rendering them robust to the noise characterizing current quantum devices.

The basis elements of the dynamical Lie algebra $\text{Lie}(A_{P\uparrow P\downarrow}^{Q\uparrow R\downarrow}, A_{P\uparrow P\downarrow}^{Q\downarrow R\uparrow})$ shown in Eq. (17) were selected be-

cause efficient quantum circuits can be constructed via the FEB framework. Nevertheless, other bases can be chosen for which efficient quantum circuits can also be devised. One such choice is the standard basis of the Lie algebra $\mathbb{R}^2 \oplus \mathfrak{so}(3)$ (see Section SIII of the Supplemental Material), whose elements are

$$\begin{aligned}\tilde{E}_1 &\equiv E_3 - E_1 \\ &= A_{P\uparrow P\downarrow}^{Q\uparrow R\downarrow} (2n_{Q\downarrow R\uparrow} - n_{Q\downarrow} - n_{R\uparrow}),\end{aligned}\quad (26)$$

$$\begin{aligned}\tilde{E}_2 &\equiv E_4 - E_2 \\ &= A_{P\uparrow P\downarrow}^{Q\downarrow R\uparrow} (2n_{Q\uparrow R\downarrow} - n_{Q\uparrow} - n_{R\downarrow}),\end{aligned}\quad (27)$$

$\tilde{E}_3 \equiv E_3$, $\tilde{E}_4 \equiv E_4$, and $\tilde{E}_5 \equiv E_5$. Using this basis and postulating the product formula

$$e^{\frac{\theta}{\sqrt{2}}(-\tilde{E}_1 + \tilde{E}_2 + \tilde{E}_3 - \tilde{E}_4)} = \prod_{i=1}^5 e^{\tilde{\alpha}_i \tilde{E}_i}, \quad (28)$$

we arrive at a corresponding Wei–Norman system that admits the following closed-form solutions:

$$\tilde{\alpha}_1(\theta) = -\frac{\theta}{\sqrt{2}}, \quad (29)$$

$$\tilde{\alpha}_2(\theta) = \frac{\theta}{\sqrt{2}}, \quad (30)$$

$$\tilde{\alpha}_3(\theta) = k\pi + \arcsin\left[\frac{\tan(\theta - k\pi)}{\sqrt{2 + \tan^2(\theta - k\pi)}}\right], \quad (31)$$

$$\tilde{\alpha}_4(\theta) = (-1)^k \arctan\left[-\frac{\tan(\theta - k\pi)}{\sqrt{2 + \tan^2(\theta - k\pi)}}\right], \quad (32)$$

and

$$\tilde{\alpha}_5(\theta) = \frac{\pi}{4} - \arctan[\cos(\theta)], \quad (33)$$

with $k = \left\lfloor \frac{\theta + \pi/2}{\pi} \right\rfloor$. Note that the piecewise-defined parameter k selects the appropriate branch of the trigonometric functions and thereby ensures continuity of the arctan terms. Furthermore, these solutions are global, *i.e.*, they hold for any value of θ , since the determinant of the corresponding Wei–Norman coefficient matrix equals $\cos(\tilde{\alpha}_4)$ and $|\arctan(x)| < \frac{\pi}{2}$.

Having discussed in detail the Wei–Norman procedure for the simpler $\exp(\theta A_{PP}^{QR})$ singlet spin-adapted unitary, we now provide the results for the decompositions of the more challenging unitaries that involve four different spatial orbitals. To facilitate the rapid derivation of error-free expressions, we developed a pilot code, build on SymPy [99], for the symbolic manipulation of fermionic

operators. Given a spin-adapted unitary as input, the code executes steps 2–5 of the Wei–Norman decomposition algorithm outlined above. For the final step, the resulting system of ordinary differential equations is integrated numerically using SciPy. Constructing the system of coupled differential equations was computationally prohibitive when the generator was ${}^{[1]}A_{PQ}^{RS}$. In this case, we employed the following strategy. First, we used our symbolic code to find a basis of the pertinent dynamical Lie algebra. We then ordered the elements by grouping them into commuting sets. Subsequently, for each value of θ , we constructed the matrix representation of the target unitary in the minimal Fock space of eight spinorbitals. The optimum values of the parameters were obtained by minimizing the Frobenius norm of the difference between the target unitary and its Wei–Norman decomposition. See Section SI of the Supplemental Material for computational details.

The spinorbital operators $A_{P\uparrow Q\downarrow}^{R\uparrow S\downarrow}$, $A_{P\downarrow Q\uparrow}^{R\downarrow S\uparrow}$, $A_{P\uparrow Q\downarrow}^{R\downarrow S\uparrow}$, and $A_{P\downarrow Q\uparrow}^{R\uparrow S\downarrow}$, which define the singlet spin-adapted generator ${}^{[0]}A_{PQ}^{RS}$ [Eq. (6)], give rise to a 28-dimensional dynamical Lie algebra. The basis elements shown in Table SI in the Supplemental Material were chosen due to the existence of efficient quantum circuit implementations. Because the number of permutations is astronomical, not only can the optimum orderings not be found by brute force, but the probability of encountering singularities is also anticipated to be high.

The ordering we selected was based on symmetry properties of the basis elements. As shown in Table SI, the 28 basis elements can be grouped into three commuting sets, containing 10, 10, and 8 operators each. The solution to the Wei–Norman system of equations is given in Fig. 3. Although we cannot guarantee that this is the best ordering, it does have various advantages. To begin with, the parameters are not rapidly varying with increasing values of the angle θ , rendering the decomposition robust to noise. Additionally, due to the aforementioned symmetries, out of the 28 parameters, only 10 are independent (see Table SI in the Supplemental Material). Finally, the basis elements $A_{P\uparrow Q\downarrow}^{P\downarrow Q\uparrow}(h_{R\uparrow R\downarrow S\uparrow S\downarrow} - n_{R\uparrow R\downarrow S\uparrow S\downarrow})$ and $A_{R\uparrow S\downarrow}^{R\downarrow S\uparrow}(h_{P\uparrow P\downarrow Q\uparrow Q\downarrow} - n_{P\uparrow P\downarrow Q\uparrow Q\downarrow})$ do not contribute to the Wei–Norman decomposition, as their parameters are numerically zero for all examined θ values. This reduces the number of exponentials from 28 down to 26, further contributing to the efficiency of the resulting quantum circuits (*vide infra*).

Similar remarks apply to the Wei–Norman decomposition of the unitary generated by the spin-adapted double excitation going through an intermediate triplet, ${}^{[1]}A_{PQ}^{RS}$ [Eq. (7)]. In this case, the basis elements of the 120-dimensional dynamical Lie algebra can be partitioned into six sets of commuting operators (see Table SII in the Supplemental Material). The solution to the pertinent Wei–Norman system of equations is given in Fig. 4. Similar to the ${}^{[0]}A_{PQ}^{RS}$ case, the parameters are slowly varying, there are only 23 independent parameters out of 120, and

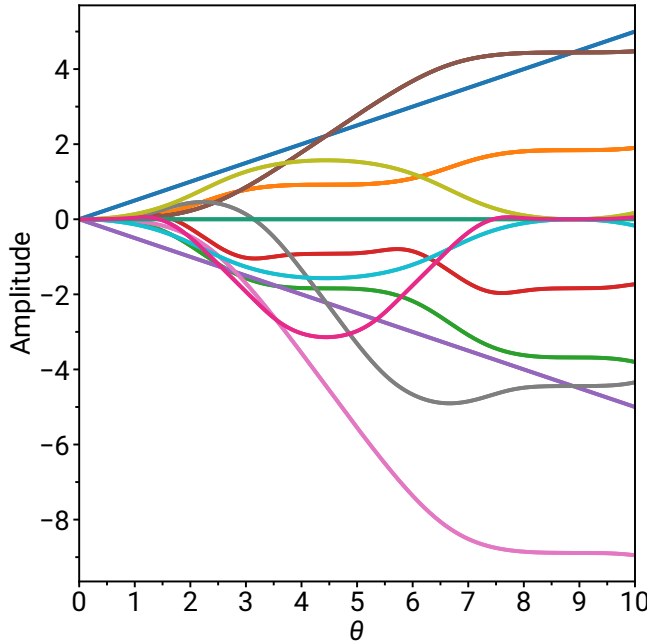


FIG. 3. Numerical values of the θ -dependent parameters defining the Wei–Norman decomposition of $\exp(\theta^{[0]}A_{PQ}^{RS})$.

six exponentials do not contribute to the Wei–Norman decomposition (see Table SII in the Supplemental Material).

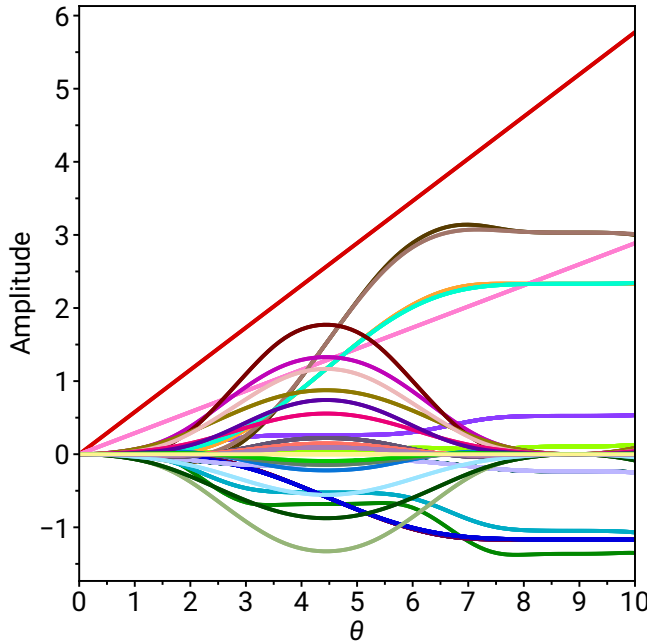


FIG. 4. Numerical values of the θ -dependent parameters defining the Wei–Norman decomposition of $\exp(\theta^{[1]}A_{PQ}^{RS})$.

Before we proceed to the discussion of circuit implementations, we mention an alternative route that may

possibly lead to exact product formulas. Let us consider, for example, the exponential $\exp[\theta(A + B)]$ with A and B being noncommuting operators. Using an m th-order Trotter–Suzuki decomposition, this exponential is approximated by a finite product of alternating exponentials of A and B [100, 101]:

$$e^{\theta(A+B)} \approx e^{\alpha_1 \theta A} e^{\alpha_2 \theta B} e^{\alpha_3 \theta A} e^{\alpha_4 \theta B} \cdots e^{\alpha_k \theta B} = e^{\theta(A+B) + \mathcal{O}(\theta^{m+1})}. \quad (34)$$

The coefficients α_i appearing in the exponentials are chosen so that all error terms up to order θ^m cancel, yielding an error of order θ^{m+1} . If the operators A and B give rise to a finite Lie algebra, it might be possible to construct an exact product formula of the form of Eq. (34), albeit with θ -dependent optimization parameters $\alpha_i(\theta)$. As shown in Section SVIII of the Supplemental Material, in the case of $\exp(\theta A_{PP}^{QR})$, we were able to find an exact product formula with six exponentials using an alternating pattern of $A_{P\uparrow P\downarrow}^{Q\uparrow R\downarrow}$ and $A_{P\uparrow P\downarrow}^{Q\uparrow R\downarrow}$ operators. However, this approach requires an additional exponential compared to the corresponding Wei–Norman decompositions. To make matters worse, the parameters are highly oscillatory functions of θ (see Fig. S15 in the Supplemental Material), rendering them more sensitive to device noise and complicating the computation of derivatives.

VI. EFFICIENT IMPLEMENTATION OF SYMMETRY-ADAPTED UNITARIES

Having presented the Wei–Norman decompositions of the unitaries generated by the singlet spin-adapted double excitation operators A_{PP}^{QR} , ${}^{[0]}A_{PQ}^{RS}$, and ${}^{[1]}A_{PQ}^{RS}$, we now proceed to the discussion of their efficient quantum circuit implementation. We begin by briefly summarizing the state-of-the-art for unitaries generated by a single anti-Hermitian, spinorbital excitation operator. As already mentioned above, such unitaries can be efficiently implemented via the FEB formalism [75, 76, 96]. Instead of translating the spinorbital generators in the qubit space via a fermionic encoding, the FEB circuits are constructed by examining the action of the entire unitary in the computational basis states. For example, consider the spinorbital double excitation $A_{P\uparrow Q\downarrow}^{R\uparrow S\downarrow}$, one of the basis elements of the dynamical Lie algebras associated with the ${}^{[0]}A_{PQ}^{RS}$ and ${}^{[1]}A_{PQ}^{RS}$ singlet spin-adapted operators. Neglecting the fermionic antisymmetry yields the qubit excitation operator $Q_{P\uparrow Q\downarrow}^{R\uparrow S\downarrow}$, with the action of the corresponding unitary being

$$e^{\theta Q_{P\uparrow Q\downarrow}^{R\uparrow S\downarrow}} \begin{pmatrix} |1_{P\uparrow}1_{Q\downarrow}0_{R\uparrow}0_{S\downarrow}\rangle \\ |0_{P\uparrow}0_{Q\downarrow}1_{R\uparrow}1_{S\downarrow}\rangle \end{pmatrix} = \begin{pmatrix} \cos \theta & \sin \theta \\ -\sin \theta & \cos \theta \end{pmatrix} \begin{pmatrix} |1_{P\uparrow}1_{Q\downarrow}0_{R\uparrow}0_{S\downarrow}\rangle \\ |0_{P\uparrow}0_{Q\downarrow}1_{R\uparrow}1_{S\downarrow}\rangle \end{pmatrix}, \quad (35)$$

acting as the identity for the remaining computational basis states. Consequently, $\exp(\theta Q_{P\uparrow Q\downarrow}^{R\uparrow S\downarrow})$ is a Givens

rotation on the plane spanned by the $|1_{P\uparrow}1_{Q\downarrow}0_{R\uparrow}0_{S\downarrow}\rangle$ and $|0_{P\uparrow}0_{Q\downarrow}1_{R\uparrow}1_{S\downarrow}\rangle$ computational basis states. The efficient, qubit excitation-based (QEB) quantum circuit representing this operation was constructed by Yordanov *et al.* [75], and is given in panel (a) of Fig. 5. In this compact form, the circuit contains 6 CNOT gates, and an $R_y(2\theta)$ gate controlled on qubit $q_{Q\downarrow}$ and anti-controlled on $q_{P\uparrow}$ and $q_{R\uparrow}$. Because fermionic signs are neglected, QEB circuits do not require CNOT staircases and, thus, act only on the qubits involved in the excitation, *i.e.*, the circuits are local. As shown in panel (b) of Fig. 5, after the decomposition of the multiqubit-controlled R_y gate, the final circuit contains 13 CNOT gates and 21 single-qubit gates [75]. From a fault-tolerant perspective, the circuit is comprised of 26 Clifford [13 CNOT, 5 H , 4 X , 2 S^\dagger , 1 S , 1 $R_y(-\frac{\pi}{2})$] and 8 non-Clifford [4 $R_y(-\frac{\theta}{4})$, 4 $R_y(\frac{\theta}{4})$] gates. The fermionic parity can be restored by “sandwiching” the circuit of Fig. 5 between two CNOT staircases and two CZ gates, marked in red color in Fig. 6. Note that in drawing the quantum circuit, we assumed that the qubit register is arranged in an alternating pattern of \uparrow and \downarrow spinorbitals. Depending on the identity of the excitation indices, the two CNOT staircases contribute $2(S\downarrow - R\uparrow + Q\downarrow - P\uparrow - 3)$ CNOTs, where $S\downarrow$, $R\uparrow$, $Q\downarrow$, and $P\uparrow$ are the spinorbital indices in the qubit register, and we assume $Q\downarrow > P\uparrow$ and $S\downarrow > R\uparrow$. This emphasizes the fact that FEB circuits, unlike their QEB counterparts, are nonlocal. Nevertheless, it is worth mentioning that restoring the fermionic parity does not introduce additional non-Clifford gates. Furthermore, in addition to fermionic antisymmetry, these quantum circuits also respect point group, particle-number, and S_z symmetries.

Adapting the above ideas to the more general generators appearing in the Wei–Norman decompositions of spin-adapted unitaries is more or less straightforward. In addition to simple spinorbital excitation operators, there are ten types of generators that can be grouped into two families of five. The first family contains generators obtained by multiplying a spinorbital double excitation operator by different linear combinations of two particle-hole-conjugate number-operator strings. Although these generators differ only in which qubits are checked by the number-operator component and how, these differences are enough to create subtle changes in the structure of the corresponding quantum circuits. As a representative example, we focus on $A_{P\uparrow Q\downarrow}^{R\uparrow S\downarrow}(h_{P\downarrow Q\uparrow} + n_{P\downarrow Q\uparrow})$. In this case, the unitary $\exp(\theta A_{P\uparrow Q\downarrow}^{R\uparrow S\downarrow})$ is applied only when $q_{P\downarrow}$ and $q_{Q\uparrow}$ are both 0 or 1, *i.e.*, when the occupancy pattern enforced by the number-operator component is satisfied. The corresponding quantum circuit is shown in Fig. 7, with the additional gates compared to Fig. 6 marked in blue. When comparing the quantum circuits of $\exp(\theta A_{P\uparrow Q\downarrow}^{R\uparrow S\downarrow})$ and $\exp(\theta A_{P\uparrow Q\downarrow}^{R\uparrow S\downarrow}(h_{P\downarrow Q\uparrow} + n_{P\downarrow Q\uparrow}))$, we notice the following differences. First, the latter has 4 fewer CNOTs in the CNOT staircases, as qubits $q_{P\downarrow}$ and $q_{Q\uparrow}$ do not contribute to the fermionic parity due

to the conditions imposed by the number-operator component. Nevertheless, two additional CNOT gates are required to check that qubits $q_{P\downarrow}$ and $q_{Q\uparrow}$ are in the same state. This results in an additional anti-control in the multiqubit-controlled R_y gate. The final circuit implementation of $\exp[\theta A_{P\uparrow Q\downarrow}^{R\uparrow S\downarrow}(h_{P\downarrow Q\uparrow} + n_{P\downarrow Q\uparrow})]$ contains 8 R_y and 6 CNOT gates more than its $\exp(\theta A_{P\uparrow Q\downarrow}^{R\uparrow S\downarrow})$ counterpart. The circuits for the remaining four generators in this family are constructed in a similar manner, by changing the location and type of the number-operator checks (see Figs. S6–S9 in the Supplemental Material).

The second family contains generators obtained by multiplying a double spin-flip operator by different linear combinations of two particle–hole-conjugate number-operator strings. A representative example in this category is $A_{P\uparrow Q\downarrow}^{P\downarrow Q\uparrow}(h_{R\uparrow S\downarrow} - n_{R\uparrow S\downarrow})$. As before, the corresponding unitary can be realized as a controlled version of $\exp(\theta A_{P\uparrow Q\downarrow}^{P\downarrow Q\uparrow})$, with one caveat. If both $R\uparrow$ and $S\downarrow$ qubits are occupied, the sign of the angle must be flipped. The quantum circuit implementing $\exp[\theta A_{P\uparrow Q\downarrow}^{P\downarrow Q\uparrow}(h_{R\uparrow S\downarrow} - n_{R\uparrow S\downarrow})]$ is shown in Fig. 8. A quick inspection of Fig. 8 immediately reveals the absence of CNOT staircases, *i.e.*, the circuit is local, a characteristic of unitaries generated by spin-flip operators whose FEB and QEB implementations coincide. Compared to $\exp(\theta A_{P\uparrow Q\downarrow}^{P\downarrow Q\uparrow})$, the quantum circuit of $\exp[\theta A_{P\uparrow Q\downarrow}^{P\downarrow Q\uparrow}(h_{R\uparrow S\downarrow} - n_{R\uparrow S\downarrow})]$ contains two additional CNOTs needed to ensure that $q_{R\uparrow} \oplus q_{S\downarrow} = 0$, resulting in an extra anti-control in the multiqubit-controlled $R_y(2\theta)$ gate. The CZ gates flip the sign of the angle θ whenever $q_{S\downarrow} = 1$. The circuits for the remaining four generators in this family are constructed in a similar manner, by changing the location and type of the number-operator checks (see Figs. S10–S13 in the Supplemental Material). The counts of CNOT and R_y gates needed to implement the types of elementary unitaries defining the Wei–Norman decompositions employed in this work are summarized in Table I.

Having presented the families of quantum circuits implementing the elementary unitaries encountered in this work, we are now in a position to provide estimates of CNOT and R_y counts characterizing the Wei–Norman decompositions of spin-adapted unitaries. Upper bounds can be readily obtained by simply adding the numbers of gates needed for the individual circuits (see Table I). In doing so, we find that $\exp(\theta A_{PP}^{QR})$, $\exp(\theta^{[0]} A_{PQ}^{RS})$, and $\exp(\theta^{[1]} A_{PQ}^{RS})$ require, at most, 64, 864, and 3696 R_y gates, respectively. As far as the number of CNOTs is concerned, we need, at most, 8 CNOT staircases and 81 CNOTs for $\exp(\theta A_{PP}^{QR})$, 40 CNOT staircases and 914 CNOTs for $\exp(\theta^{[0]} A_{PQ}^{RS})$, and 144 CNOT staircases and 4134 CNOTs in the case of $\exp(\theta^{[1]} A_{PQ}^{RS})$. These estimates, however, are rather pessimistic, as various sim-

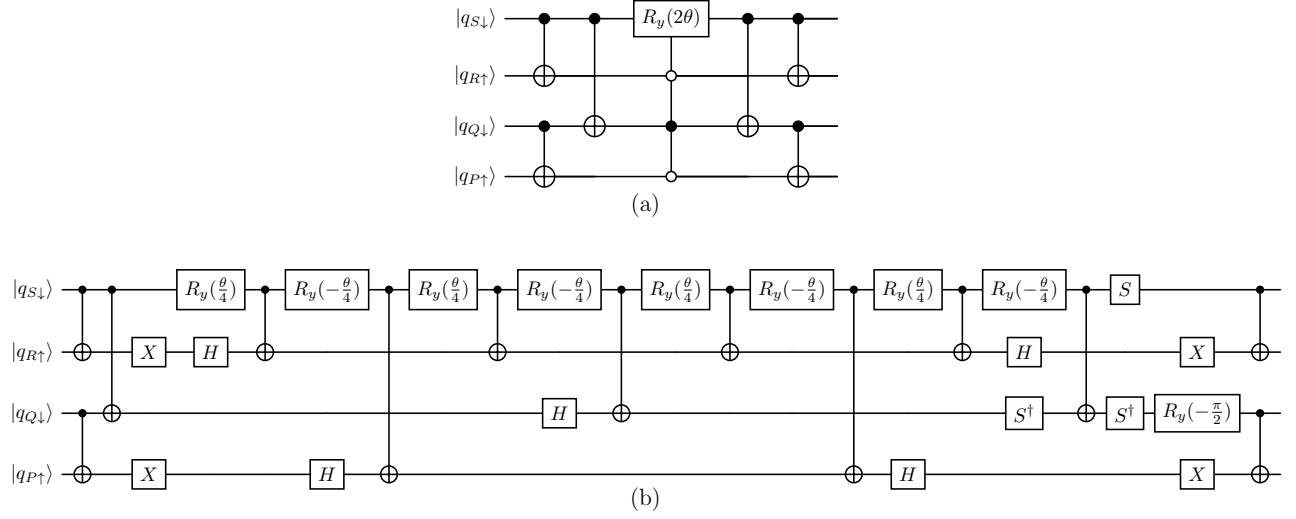


FIG. 5. Qubit excitation-based circuit implementing the unitary $\exp(\theta Q_{P↑Q↓}^{R↑S↓})$. In (b), the multiqubit-controlled R_y gate of (a) has been decomposed.

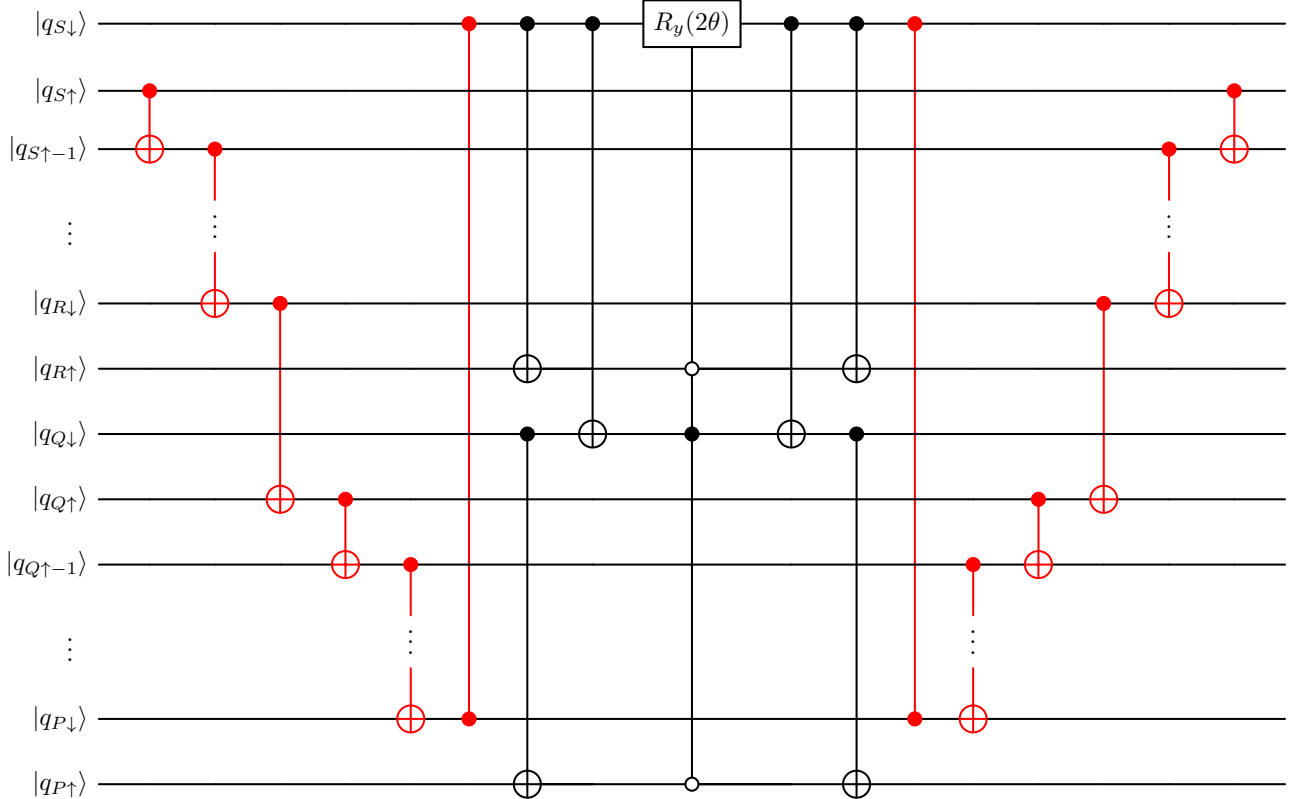


FIG. 6. Fermionic excitation-based quantum circuit implementing the unitary $\exp(\theta A_{P↑Q↓}^{R↑S↓})$.

plifications are possible. We anticipate that by canceling adjacent CNOTs/CNOT staircases, the implementations of $\exp(\theta A_{PP}^{QR})$, $\exp(\theta [0]A_{PQ}^{RS})$, and $\exp(\theta [1]A_{PQ}^{RS})$ would more or less require 2 CNOT staircases and 60 CNOTs, 2 CNOT staircases and 750 CNOTs, and 8 CNOT staircases and 3600 CNOTs, respectively. Although these are rough estimates and there is still room for further optimizations, they do provide a baseline for gauging the amount of quantum resources needed to exactly implemented unitaries generated by singlet spin-adapted double excitation operators.

VII. MINIMUM UNIVERSAL SYMMETRY-ADAPTED OPERATOR POOL

By designing efficient quantum circuits for unitaries generated by the saGSD pool, we have enabled the hardware implementation of symmetry-preserving quantum simulations for many-fermion systems. An open question is how to further reduce the required computational resources. As anticipated purely on the number of exponentials, the dominant contributor to the computational cost is the unitary generated by $[1]A_{PQ}^{RS}$, whose quantum circuit implementation requires approximately five times as many CNOT gates and four times as many CNOT staircases as its $[0]A_{PQ}^{RS}$ counterpart. Although it seems unlikely that more aggressive circuit optimizations would lower the CNOT count by a few thousand gates, one can question whether this type of generator is required to attain universality. Indeed, for molecules without spatial symmetry, *i.e.*, those in the C_1 point group, and with not all electrons with \uparrow or \downarrow spin, it has been shown that the saGSpD pool, which is comprised of singlet spin-adapted singles and perfect pairing doubles, is universal [51]. To retain expressivity for systems with higher spatial symmetry, non-totally symmetric spin-adapted single excitations are typically included in the pool [50–52], albeit introducing spatial symmetry contaminants. An alternative route to universality, while still enforcing all symmetries, is to augment the saGSpD pool with additional types of singlet spin-adapted double excitation operators. Considering that the A_{PP}^{QR} operators are implicitly included in the saGSpD pool via the commutator identity $A_{PP}^{QR} = [A_{QQ}^{PP}, A_Q^R]$, it is worth examining the universality of approximations to saGSD that incorporate the $[0]A_{PQ}^{RS}$ operators.

To that end, we performed preliminary numerical simulations for the ground, 1A_g , electronic state of a D_{2h} -symmetric distorted hexagonal arrangement of six hydrogen atoms in the STO-6G minimum basis [102] (see Section SVII of the Supplemental Material for the nuclear coordinates). We employed the adaptive derivative-assembled pseudo-Trotter (ADAPT) [18] variational quantum eigensolver (VQE) [103]. We considered the GSD pool, which conserves all symmetries except S^2 , and the saGSD pool and several of its approximations de-

fined in panel (a) of Fig. 9, all of which respect all symmetries. In each ADAPT-VQE macro-iteration, we selected the operator with the largest energy gradient from the corresponding pool and appended it to the ansatz. The simulations were terminated when the ansatz contained as many parameters as the dimension of the corresponding many-electron Hilbert space minus one (to account for normalization). During the VQE steps, all parameters were optimized variationally using the Broyden–Fletcher–Goldfarb–Shanno (BFGS) optimizer [104–107], as implemented in SciPy. The convergence criterion for the micro-iterations was set to $10^{-6} E_h$ for the gradient norm. All numerical simulations were performed using a developmental version of QForte [108] and employed one- and two-electron integrals obtained with restricted Hartree–Fock (RHF) as implemented in Psi4 [109].

In Fig. 9, we show the results of our ADAPT-VQE numerical simulations for the H_6 /STO-6G system. We begin by noticing that although ADAPT-VQE-GSD eventually collapsed to the exact ground electronic state, it requires an unnecessarily large number of parameters, as it is exploring the much larger 6-electron Hilbert space containing totally symmetric, $S_z = 0$ singlet, triplet, quintet, and septet states. Indeed, as shown in panel (c) of Fig. 9, the ADAPT-VQE-GSD simulation is plagued by severe spin-symmetry breaking, which is eventually restored as the wavefunction collapses to the lowest-energy 1A_g state. When employing the saGSD pool, ADAPT-VQE provides chemically accurate results (within $1 mE_h$ of the exact energy) with almost one third of the parameters compared to its GSD counterpart, and produces numerically exact energies with about half the number of parameters. However, the saGSD pool contains all types of singlet spin-adapted double excitations, including the quantum-resource-demanding $[1]A_{PQ}^{RS}$ ones.

Although all approximations to the saGSD pool explored in this study rigorously enforce all symmetries, they may not be as expressive as the parent pool. A characteristic example is the CNOT-frugal saGSpD pool, which is not universal when point-group symmetry is enforced and barely improves upon the underlying RHF energy. The two approximations to saGSD that produce numerically exact energies are saGSD0 and pDint0. As shown in panel (a) of Fig. 9, the saGSD0 pool is reminiscent of the classical CCD0 and CCSD0 approaches [110], while pDint0 contains only perfect-pairing doubles and spin-adapted doubles going through an intermediate singlet. Although both pools have the same cost in terms of CNOTs, namely, the $[0]A_{PQ}^{RS}$ operators, pDint0 contains fewer elements, resulting in a reduced number of measurements required for the expansion step of adaptive algorithms such as ADAPT-VQE. Based on these preliminary numerical results, pDint0 is the smallest universal symmetry-adapted operator pool, striking the best balance between computational cost and rigorously enforcing all symmetries.

Before concluding, we note how the symmetry-adapted quantum circuits presented in this work can be deployed

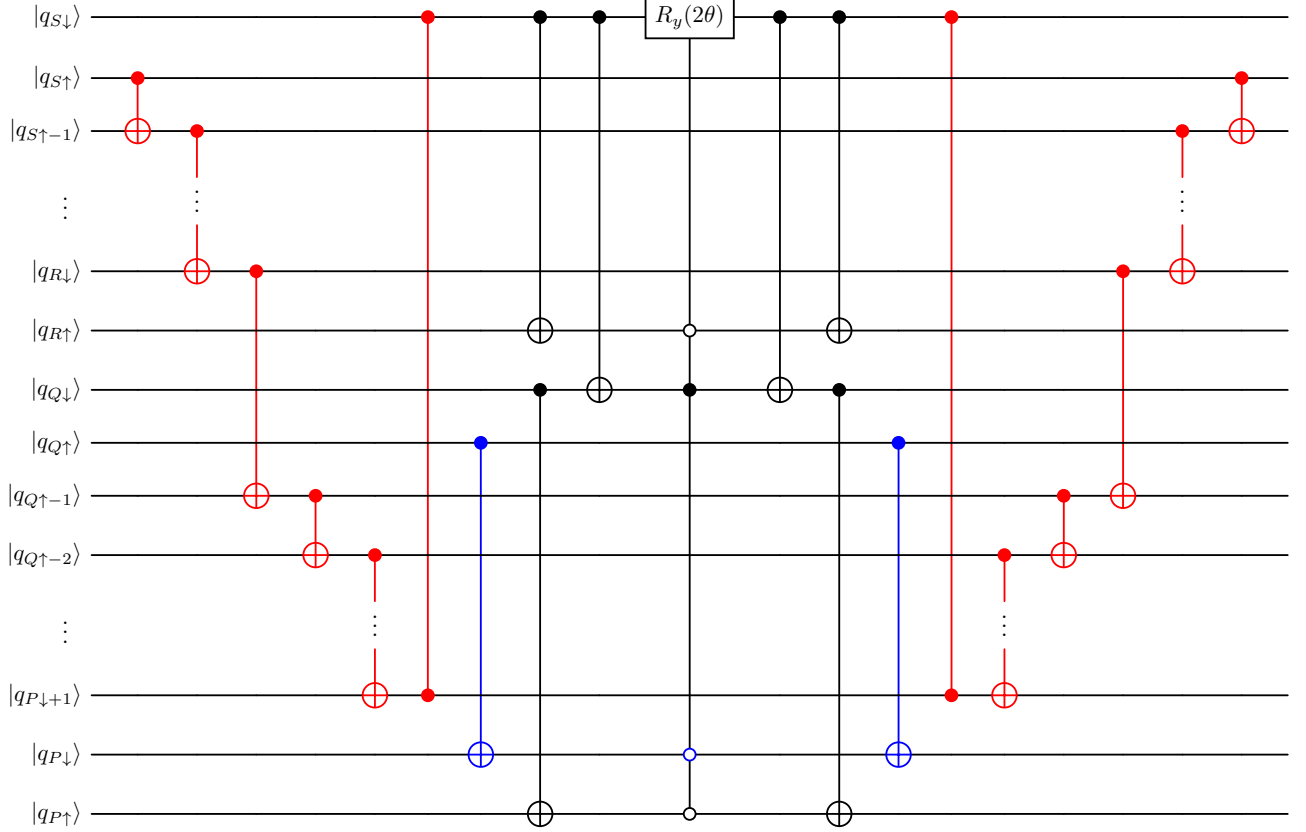


FIG. 7. Fermionic excitation-based quantum circuit implementing $\exp\left[\theta A_{P\uparrow Q\downarrow}^{R\uparrow S\downarrow}(h_{P\downarrow Q\uparrow} + n_{P\downarrow Q\uparrow})\right]$.

TABLE I. Numbers of CNOT and R_y gates required by the fermionic excitation-based quantum circuits of Figs. 6 to 8 and Figs. S6–S13 in the Supplemental Material.

generator	CNOT Count ^a	R_y Count
$A_{P\uparrow Q\downarrow}^{R\uparrow S\downarrow}$	$2(S\downarrow - R\uparrow + Q\downarrow - P\uparrow) + 9$	8
$A_{P\uparrow Q\downarrow}^{R\uparrow S\downarrow}(h_{P\downarrow Q\uparrow} + n_{P\downarrow Q\uparrow})$	$2(S\downarrow - R\uparrow + Q\downarrow - P\uparrow) + 15$	16
$A_{P\uparrow Q\downarrow}^{R\uparrow S\downarrow}(n_{Q\uparrow}h_{S\uparrow} + h_{Q\uparrow}n_{S\uparrow})$	$2(S\downarrow - R\uparrow + Q\downarrow - P\uparrow) + 15$	16
$A_{P\uparrow Q\downarrow}^{R\uparrow S\downarrow}(h_{P\downarrow Q\uparrow}n_{S\uparrow} + n_{P\downarrow Q\uparrow}h_{S\uparrow})$	$2(S\downarrow - R\uparrow + Q\downarrow - P\uparrow) + 33$	32
$A_{P\uparrow Q\downarrow}^{R\uparrow S\downarrow}(h_{P\downarrow Q\uparrow}R\downarrow S\uparrow + n_{P\downarrow Q\uparrow}R\downarrow S\uparrow)$	$2(S\downarrow - R\uparrow + Q\downarrow - P\uparrow) + 63$	64
$A_{P\uparrow Q\downarrow}^{R\uparrow S\downarrow}(h_{P\downarrow Q\uparrow}n_{R\downarrow S\uparrow} + n_{P\downarrow Q\uparrow}h_{R\downarrow S\uparrow})$	$2(S\downarrow - R\uparrow + Q\downarrow - P\uparrow) + 63$	64
$A_{P\uparrow Q\downarrow}^{R\uparrow S\downarrow}(h_{R\uparrow S\downarrow} - n_{R\uparrow S\downarrow})$	25	16
$A_{Q\uparrow R\downarrow}^{R\uparrow S\downarrow}(h_{P\uparrow}n_{S\uparrow} - n_{P\uparrow}h_{S\uparrow})$	25	16
$A_{P\uparrow Q\downarrow}^{R\uparrow S\downarrow}(h_{R\uparrow S\downarrow}n_{S\uparrow} - n_{R\uparrow S\downarrow}h_{S\uparrow})$	43	32
$A_{P\uparrow Q\downarrow}^{R\uparrow S\downarrow}(h_{R\uparrow}R\downarrow S\uparrow S\downarrow - n_{R\uparrow}R\downarrow S\uparrow S\downarrow)$	77	64
$A_{P\uparrow Q\downarrow}^{R\uparrow S\downarrow}(h_{R\uparrow}S\downarrow n_{R\downarrow}S\uparrow - n_{R\uparrow}S\downarrow h_{R\downarrow}S\uparrow)$	77	64

^a The given CNOT counts include CZ gates, as they can be converted into CNOTs.

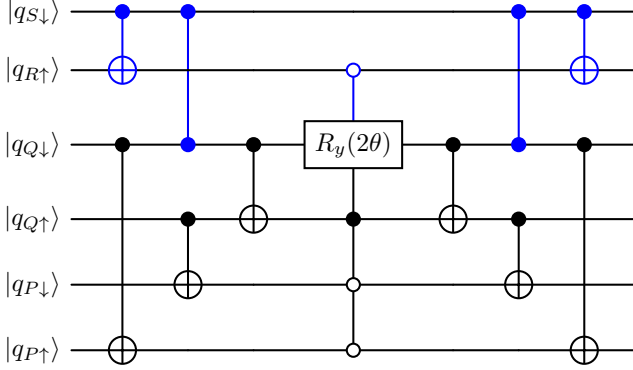


FIG. 8. Fermionic excitation-based quantum circuit implementing $\exp[\theta A_{P\uparrow Q\downarrow}^{PQ} (h_{R\uparrow S\downarrow} - n_{R\uparrow S\downarrow})]$.

on actual hardware. As shown in Figs. 2 to 4, most parameters appearing in the Wei–Norman decompositions of the singlet spin-adapted unitaries $\exp(\theta A_{PP}^{QR})$, $\exp(\theta [0]A_{PQ}^{RS})$, and $\exp(\theta [1]A_{PQ}^{RS})$ do not admit simple analytic expressions. Nevertheless, by construction, they are continuous and differentiable. Consequently, these unitaries can be employed in ADAPT-VQE experiments, similar to the numerical simulations presented in Fig. 9. We have tabulated all parameter values on a dense grid of θ with step-size 0.005. These data could be used to interpolate between points as needed. Gradients with respect to θ required for VQE simulations can then be computed exactly via the parameter-shift rule [111–114], while evaluating the shifted circuits using the tabulated/interpolated parameters. It is worth mentioning that for numerical simulations, the closed-form expressions reported in Refs. [17, 85] are the most efficient implementations of unitaries generated by singlet spin-adapted double excitation operators.

VIII. CONCLUSIONS

In this work, we introduced computationally efficient quantum circuits that rigorously enforce all symmetries relevant to chemistry applications, including point-group, particle-number, S_z , and S^2 . Specifically, we derived exact product formulas for unitaries generated by singlet spin-adapted double excitation operators via the Wei–Norman decomposition. For each elementary unitary in these decompositions, we constructed CNOT-efficient circuits based on the fermionic excitation-based formalism. The total number of R_y gates are 64, 864, and 3696 for the $\exp(\theta A_{PP}^{QR})$, $\exp(\theta [0]A_{PQ}^{RS})$, and $\exp(\theta [1]A_{PQ}^{RS})$ unitaries, respectively. The corresponding two-qubit gate costs are estimated to be 2 CNOT staircases plus 60 CNOTs for $\exp(\theta A_{PP}^{QR})$, 2 CNOT staircases plus 750 CNOTs for $\exp(\theta [0]A_{PQ}^{RS})$, and 8 CNOT staircases plus

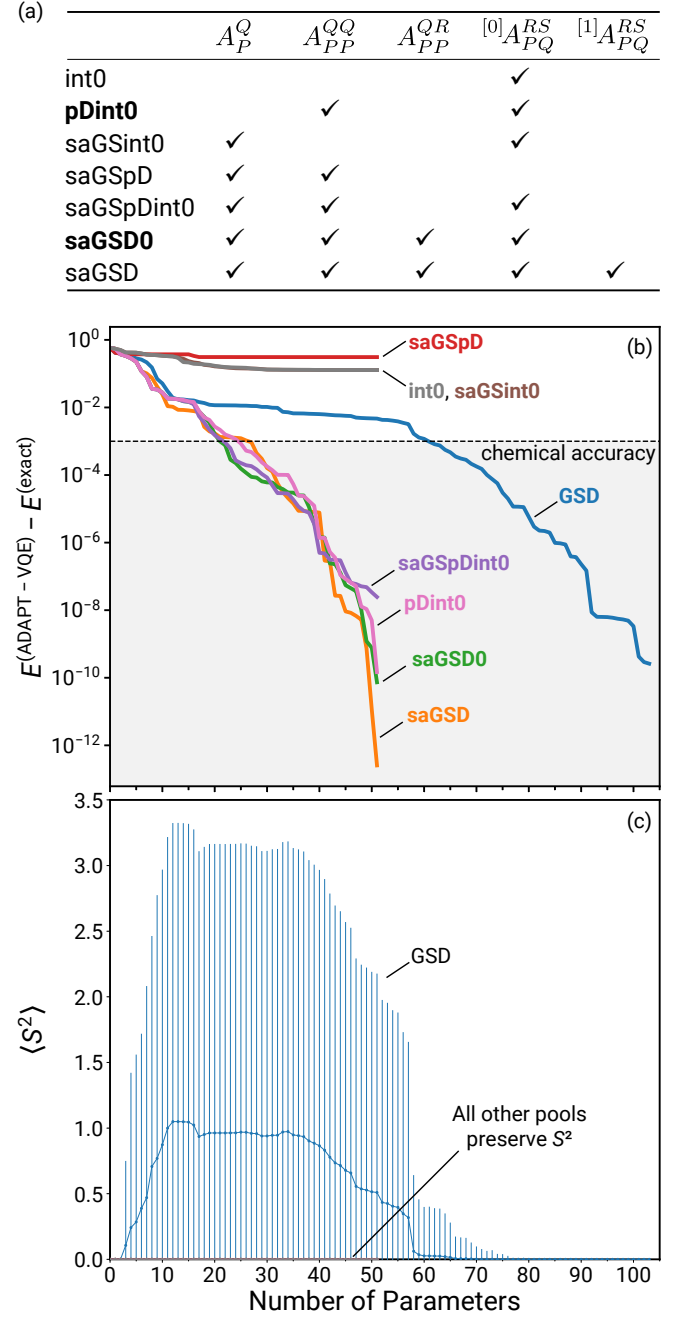


FIG. 9. ADAPT-VQE simulations using the GSD and several spin-adapted operator pools for the D_{2h} -symmetric distorted hexagonal H_6 /STO-6G system. (a) Definitions of the spin-adapted operator pools, (b) errors relative to the exact energy of the ground 1A_g electronic state, and (c) expectation values of the total spin squared S^2 operator (the vertical lines denote standard deviations, computed as $\sigma_A = \sqrt{\langle A^2 \rangle - \langle A \rangle^2}$).

3600 CNOTs in the case of $\exp(\theta [1]A_{PQ}^{RS})$. Furthermore, our Wei–Norman decompositions are also compatible with the parameter-shift rule for gradient evaluations, enabling their deployment on quantum hardware.

We presented numerical evidence supporting the conjecture that a pool of perfect-pairing doubles and doubles going through an intermediate singlet is universal while preserving all symmetries. Compared with the full singlet spin-adapted singles and doubles pool, this choice dramatically reduces the computational cost, while overcoming the limitations of the more affordable operator pool containing singlet spin-adapted singles and perfect pairing doubles. As a result, the intermediate-singlet pool offers the best balance between computational efficiency

and rigorous enforcement of all symmetries relevant to chemistry applications.

ACKNOWLEDGMENTS

The authors would like to thank Mr. Muhan Zhang for insightful discussions regarding the quantum circuits presented in this study. This work was supported by the U.S. Department of Energy under Award No. DE-SC0019374.

[1] R. P. Feynman, Simulating physics with computers, *Int. J. Theor. Phys.* **21**, 467 (1982).

[2] S. Lloyd, Universal quantum simulators, *Science* **273**, 1073 (1996).

[3] I. M. Georgescu, S. Ashhab, and F. Nori, Quantum simulation, *Rev. Mod. Phys.* **86**, 153 (2014).

[4] M. Reiher, N. Wiebe, K. M. Svore, D. Wecker, and M. Troyer, Elucidating reaction mechanisms on quantum computers, *Proc. Natl. Acad. Sci. U.S.A.* **114**, 7555 (2017).

[5] J. Paldus, Group theoretical approach to the configuration interaction and perturbation theory calculations for atomic and molecular systems, *J. Chem. Phys.* **61**, 5321 (1974).

[6] D. S. Abrams and S. Lloyd, Simulation of many-body Fermi systems on a universal quantum computer, *Phys. Rev. Lett.* **79**, 2586 (1997).

[7] D. S. Abrams and S. Lloyd, Quantum algorithm providing exponential speed increase for finding eigenvalues and eigenvectors, *Phys. Rev. Lett.* **83**, 5162 (1999).

[8] D. W. Berry, G. Ahokas, R. Cleve, and B. C. Sanders, Efficient quantum algorithms for simulating sparse Hamiltonians, *Commun. Math. Phys.* **270**, 359 (2007).

[9] R. Babbush, N. Wiebe, J. McClean, J. McClain, H. Neven, and G. K.-L. Chan, Low-depth quantum simulations of materials, *Phys. Rev. X* **8**, 011044 (2018).

[10] Y. Cao, J. Romero, J. P. Olson, M. Degroote, P. D. Johnson, M. Kieferová, I. D. Kivlichan, T. Menke, B. Peropadre, N. P. D. Sawaya, S. Sim, L. Veis, and A. Aspuru-Guzik, Quantum chemistry in the age of quantum computing, *Chem. Rev.* **119**, 10856 (2019).

[11] B. Bauer, S. Bravyi, M. Motta, and G. K.-L. Chan, Quantum algorithms for quantum chemistry and quantum materials science, *Chem. Rev.* **120**, 12685 (2020).

[12] S. McArdle, S. Endo, A. Aspuru-Guzik, S. C. Benjamin, and X. Yuan, Quantum computational chemistry, *Rev. Mod. Phys.* **92**, 015003 (2020).

[13] Z. Cai, R. Babbush, S. C. Benjamin, S. Endo, W. J. Huggins, Y. Li, J. R. McClean, and T. E. O’Brien, Quantum error mitigation, *Rev. Mod. Phys.* **95**, 045005 (2023).

[14] S. Aaronson, Quantum computing, postselection, and probabilistic polynomial-time, *Proc. R. Soc. A* **461**, 3473 (2005).

[15] X. Bonet-Monroig, R. Sagastizabal, M. Singh, and T. E. O’Brien, Low-cost error mitigation by symmetry verification, *Phys. Rev. A* **98**, 062339 (2018).

[16] S. McArdle, X. Yuan, and S. Benjamin, Error-mitigated digital quantum simulation, *Phys. Rev. Lett.* **122**, 180501 (2019).

[17] I. Magoulas and F. A. Evangelista, Closed-form expressions for unitaries of spin-adapted fermionic operators, *Mol. Phys.* **1**, e2534672 (2025).

[18] H. R. Grimsley, S. E. Economou, E. Barnes, and N. J. Mayhall, An adaptive variational algorithm for exact molecular simulations on a quantum computer, *Nat. Commun.* **10**, 3007 (2019).

[19] I. G. Ryabinkin, R. A. Lang, S. N. Genin, and A. F. Izmaylov, Iterative qubit coupled cluster approach with efficient screening of generators, *J. Chem. Theory Comput.* **16**, 1055 (2020).

[20] N. H. Stair and F. A. Evangelista, Simulating many-body systems with a projective quantum eigensolver, *PRX Quantum* **2**, 030301 (2021).

[21] J. Wei and E. Norman, Lie algebraic solution of linear differential equations, *J. Math. Phys.* **4**, 575 (1963).

[22] J. Wei and E. Norman, On global representations of the solutions of linear differential equations as a product of exponentials, *Proc. Am. Math. Soc.* **15**, 327 (1964).

[23] J. D. Whitfield, Commutation: Spin-free quantum computational simulations and symmetry adapted states, *J. Chem. Phys.* **139**, 021105 (2013).

[24] A. F. Izmaylov, On construction of projection operators, *J. Phys. Chem. A* **123**, 3429 (2019).

[25] K. Seki, T. Shirakawa, and S. Yunoki, Symmetry-adapted variational quantum eigensolver, *Phys. Rev. A* **101**, 052340 (2020).

[26] K. Seki and S. Yunoki, Spatial, spin, and charge symmetry projections for a Fermi-Hubbard model on a quantum computer, *Phys. Rev. A* **105**, 032419 (2022).

[27] T. Tsuchimochi, Y. Mori, and S. L. Ten-no, Spin projection for quantum computation: A low-depth approach to strong correlation, *Phys. Rev. Res.* **2**, 043142 (2020).

[28] T. Tsuchimochi, M. Taiji, T. Nishimaki, and S. L. Ten-no, Adaptive construction of shallower quantum circuits with quantum spin projection for fermionic systems, *Phys. Rev. Research* **4**, 033100 (2022).

[29] P. Siwach and D. Lacroix, Filtering states with total spin on a quantum computer, *Phys. Rev. A* **104**, 062435 (2021).

[30] E. A. R. Guzman and D. Lacroix, Restoring broken symmetries using quantum search “oracles”, *Phys. Rev. C* **107**, 034310 (2023).

[31] A. Khamoshi, F. A. Evangelista, and G. E. Scuseria, Correlating AGP on a quantum computer, *Quantum*

Sci. Technol. **6**, 014004 (2021).

[32] E. A. R. Guzman and D. Lacroix, Accessing ground-state and excited-state energies in a many-body system after symmetry restoration using quantum computers, *Phys. Rev. C* **105**, 024324 (2022).

[33] A. M. Childs and N. Wiebe, Hamiltonian simulation using linear combinations of unitary operations, *Quantum Inform. Comput.* **12**, 901 (2012).

[34] D. W. Berry, A. M. Childs, R. Cleve, R. Kothari, and R. D. Somma, Simulating hamiltonian dynamics with a truncated taylor series, *Phys. Rev. Lett.* **114**, 090502 (2015).

[35] J. R. McClean, J. Romero, R. Babbush, and A. Aspuru-Guzik, The theory of variational hybrid quantum-classical algorithms, *New J. Phys.* **18**, 023023 (2016).

[36] I. G. Ryabinkin, S. N. Genin, and A. F. Izmaylov, Constrained variational quantum eigensolver: Quantum computer search engine in the fock space, *J. Chem. Theory Comput.* **15**, 249 (2019).

[37] G. Greene-Diniz and D. M. Ramo, Generalized unitary coupled cluster excitations for multireference molecular states optimized by the variational quantum eigensolver, *Int. J. Quantum Chem.* **121**, e26352 (2021).

[38] K. Kuroiwa and Y. O. Nakagawa, Penalty methods for a variational quantum eigensolver, *Phys. Rev. Research* **3**, 013197 (2021).

[39] R. Selvarajan, M. Sajian, and S. Kais, Variational quantum circuits to prepare low energy symmetry states, *Symmetry* **14**, 457 (2022).

[40] S. Bravyi, J. M. Gambetta, A. Mezzacapo, and K. Temme, *Tapering off qubits to simulate fermionic Hamiltonians* (2017), arXiv:1701.08213 [quant-ph].

[41] K. Setia, R. Chen, J. E. Rice, A. Mezzacapo, M. Pistoia, and J. D. Whitfield, Reducing qubit requirements for quantum simulations using molecular point group symmetries, *J. Chem. Theory Comput.* **16**, 6091 (2020).

[42] D. Picozzi and J. Tennyson, Symmetry-adapted encodings for qubit number reduction by point-group and other boolean symmetries, *Quantum Sci. Technol.* **8**, 035026 (2023).

[43] K. Sugisaki, S. Yamamoto, S. Nakazawa, K. Toyota, K. Sato, D. Shiomi, and T. Takui, Quantum chemistry on quantum computers: A polynomial-time quantum algorithm for constructing the wave functions of open-shell molecules, *J. Phys. Chem. A* **120**, 6459 (2016).

[44] K. Sugisaki, S. Yamamoto, S. Nakazawa, K. Toyota, K. Sato, D. Shiomi, and T. Takui, Open shell electronic state calculations on quantum computers: A quantum circuit for the preparation of configuration state functions based on serber construction, *Chem. Phys. Lett.* **737**, 100002 (2019).

[45] B. T. Gard, L. Zhu, G. S. Baron, N. J. Mayhall, S. E. Economou, and E. Barnes, Efficient symmetry-preserving state preparation circuits for the variational quantum eigensolver algorithm, *npj Quantum Information* **6**, 10 (2020).

[46] A. Carbone, D. E. Galli, M. Motta, and B. Jones, Quantum circuits for the preparation of spin eigenfunctions on quantum computers, *Symmetry* **14**, 624 (2022).

[47] A. Y. Kitaev, Quantum measurements and the abelian stabilizer problem, 1995, arXiv:quant-ph/9511026. arXiv.org e-Print archive. <https://arxiv.org/abs/quant-ph/9511026>.

[48] D. Bacon, I. L. Chuang, and A. W. Harrow, Efficient quantum circuits for Schur and Clebsch-Gordan transforms, *Phys. Rev. Lett.* **97**, 170502 (2006).

[49] A. Gandon, A. Baiardi, M. Rossmannek, W. Dobrautz, and I. Tavernelli, Quantum computing in spin-adapted representations for efficient simulations of spin systems, *PRX Quantum* **6**, 030306 (2025).

[50] G.-L. R. Anselmetti, D. Wierichs, C. Gogolin, and R. M. Parrish, Local, expressive, quantum-number-preserving vqe ansätze for fermionic systems, *New J. Phys.* **23**, 113010 (2021).

[51] H. G. A. Burton, D. Marti-Dafcik, D. P. Tew, and D. J. Wales, Exact electronic states with shallow quantum circuits from global optimisation, *npj Quantum Inf.* **9**, 75 (2023).

[52] H. G. A. Burton, Accurate and gate-efficient quantum ansätze for electronic states without adaptive optimisation, *Phys. Rev. Research* **6**, 023300 (2024).

[53] W. Kutzelnigg, in *Methods of Electronic Structure Theory*, edited by H. F. Schaefer, III (Springer, Boston, 1977) pp. 129–188.

[54] W. Kutzelnigg, Quantum chemistry in Fock space. I. The universal wave and energy operators, *J. Chem. Phys.* **77**, 3081 (1982).

[55] W. Kutzelnigg and S. Koch, Quantum chemistry in Fock space. II. Effective Hamiltonians in Fock space, *J. Chem. Phys.* **79**, 4315 (1983).

[56] W. Kutzelnigg, Quantum chemistry in Fock space. III. Particle-hole formalism, *J. Chem. Phys.* **80**, 822 (1984).

[57] R. J. Bartlett, S. A. Kucharski, and J. Noga, Alternative coupled-cluster ansätze II. The unitary coupled-cluster method, *Chem. Phys. Lett.* **155**, 133 (1989).

[58] P. G. Szalay, M. Nooijen, and R. J. Bartlett, Alternative ansätze in single reference coupled-cluster theory. III. A critical analysis of different methods, *J. Chem. Phys.* **103**, 281 (1995).

[59] A. G. Taube and R. J. Bartlett, New perspectives on unitary coupled-cluster theory, *Int. J. Quantum Chem.* **106**, 3393 (2006).

[60] B. Cooper and P. J. Knowles, Benchmark studies of variational, unitary and extended coupled cluster methods, *J. Chem. Phys.* **133**, 234102 (2010).

[61] F. A. Evangelista, Alternative single-reference coupled cluster approaches for multireference problems: The simpler, the better, *J. Chem. Phys.* **134**, 224102 (2011).

[62] G. Harsha, T. Shiozaki, and G. E. Scuseria, On the difference between variational and unitary coupled cluster theories, *J. Chem. Phys.* **148**, 044107 (2018).

[63] M.-A. Filip and A. J. W. Thom, A stochastic approach to unitary coupled cluster, *J. Chem. Phys.* **153**, 214106 (2020).

[64] J. K. Freericks, Operator relationship between conventional coupled cluster and unitary coupled cluster, *Symmetry* **14**, 494 (2022).

[65] A. Anand, P. Schleich, S. Alperin-Lea, P. W. K. Jensen, S. Sim, M. Díaz-Tinoco, J. S. Kottmann, M. Degroote, A. F. Izmaylov, and A. Aspuru-Guzik, A quantum computing view on unitary coupled cluster theory, *Chem. Soc. Rev.* **51**, 1659 (2022).

[66] F. Coester, Bound states of a many-particle system, *Nucl. Phys.* **7**, 421 (1958).

[67] F. Coester and H. Kümmel, Short-range correlations in nuclear wave functions, *Nucl. Phys.* **17**, 477 (1960).

[68] J. Čížek, On the correlation problem in atomic and molecular systems. Calculation of wavefunction components in Ursell-type expansion using quantum-field theoretical methods, *J. Chem. Phys.* **45**, 4256 (1966).

[69] J. Čížek, On the use of the cluster expansion and the technique of diagrams in calculations of correlation effects in atoms and molecules, *Adv. Chem. Phys.* **14**, 35 (1969).

[70] J. Čížek and J. Paldus, Correlation problems in atomic and molecular systems III. Rederivation of the coupled-pair many-electron theory using the traditional quantum chemical methods, *Int. J. Quantum Chem.* **5**, 359 (1971).

[71] J. Paldus, J. Čížek, and I. Shavitt, Correlation problems in atomic and molecular systems. IV. Extended coupled-pair many-electron theory and its application to the BH_3 molecule, *Phys. Rev. A* **5**, 50 (1972).

[72] M. Nooijen, Can the eigenstates of a many-body Hamiltonian be represented exactly using a general two-body cluster expansion?, *Phys. Rev. Lett.* **84**, 2108 (2000).

[73] H. Nakatsuji, Structure of the exact wave function, *J. Chem. Phys.* **113**, 2949 (2000).

[74] F. A. Evangelista, G. K.-L. Chan, and G. E. Scusearia, Exact parameterization of fermionic wave functions via unitary coupled cluster theory, *J. Chem. Phys.* **151**, 244112 (2019).

[75] Y. S. Yordanov, D. R. M. Arvidsson-Shukur, and C. H. W. Barnes, Efficient quantum circuits for quantum computational chemistry, *Phys. Rev. A* **102**, 062612 (2020).

[76] R. Xia and S. Kais, Qubit coupled cluster singles and doubles variational quantum eigensolver ansatz for electronic structure calculations, *Quantum Sci. Technol.* **6**, 015001 (2021).

[77] J. Paldus, B. G. Adams, and J. Čížek, *Int. J. Quantum Chem.* **11**, 813 (1977).

[78] J. Paldus, *J. Chem. Phys.* **67**, 303 (1977).

[79] B. G. Adams and J. Paldus, *Phys. Rev. A* **20**, 1 (1979).

[80] R. A. Chiles and C. E. Dykstra, *J. Chem. Phys.* **74**, 4544 (1981).

[81] P. Piecuch and J. Paldus, *Int. J. Quantum Chem.* **36**, 429 (1989).

[82] J. Geertsen, S. Eriksen, and J. Oddershede, *Adv. Quantum Chem.* **22**, 167 (1991).

[83] P. Piecuch and J. Paldus, *Theor. Chim. Acta* **83**, 69 (1992).

[84] P. Piecuch and J. Paldus, *J. Chem. Phys.* **101**, 5875 (1994).

[85] E. R. Kjellgren, K. M. Ziems, P. Reinholdt, S. P. A. Sauer, S. Coriani, and J. Kongsted, Exact closed-form expressions for unitary spin-adapted fermionic singlet double excitation operators, *J. Chem. Phys.* **163**, 134115 (2025).

[86] P. Jordan and E. Wigner, Über das Paulische Äquivalenzverbot, *Z. Phys.* **47**, 631 (1928).

[87] S. B. Bravyi and A. Y. Kitaev, Fermionic quantum computation, *Ann. Phys.* **298**, 210 (2002).

[88] D. W. Berry, A. M. Childs, R. Cleve, R. Kothari, and R. D. Somma, Exponential improvement in precision for simulating sparse Hamiltonians, in *Proceedings of the Forty-Sixth Annual ACM Symposium on Theory of Computing*, STOC '14 (Association for Computing Machinery, New York, NY, USA, 2014) pp. 283–292.

[89] D. W. Berry, A. M. Childs, and R. Kothari, Hamiltonian simulation with nearly optimal dependence on all parameters, in *2015 IEEE 56th Annual Symposium on Foundations of Computer Science* (2015) pp. 792–809.

[90] A. Gilyén, Y. Su, G. H. Low, and N. Wiebe, Quantum singular value transformation and beyond: Exponential improvements for quantum matrix arithmetics, in *Proceedings of the 51st Annual ACM SIGACT Symposium on Theory of Computing*, STOC 2019 (2019) pp. 193–204.

[91] G. H. Low and I. L. Chuang, Optimal hamiltonian simulation by quantum signal processing, *Phys. Rev. Lett.* **118**, 010501 (2017).

[92] G. H. Low and I. L. Chuang, Hamiltonian simulation by qubitization, *Quantum* **3**, 163 (2019).

[93] C. Altafini, Use of Wei–Norman formulæ and parameter differentiation in quantum computing, in *Proceedings of the 15th International Symposium on Mathematical Theory of Networks and Systems (MTNS 2002)* (University of Notre Dame, South Bend, IN, USA) 6 pages.

[94] S. Charzyński and M. Kuś, Wei–Norman equations for a unitary evolution, *J. Phys. A: Math. Theor.* **46**, 265208 (2013).

[95] F. A. Evangelista and I. Magoulas, Exact Closed-Form Unitary Transformations of Fermionic Operators, *Phys. Rev. A* **111**, 042825 (2025).

[96] I. Magoulas and F. A. Evangelista, CNOT-efficient circuits for arbitrary rank many-body fermionic and qubit excitations, *J. Chem. Theory Comput.* **19**, 822 (2023).

[97] P. Virtanen, R. Gommers, T. E. Oliphant, M. Haberland, T. R. Amd D. Cournapeau, E. Burovski, P. Peterson, W. Weckesser, J. Bright, S. J. van der Walt, M. Brett, J. Wilson, K. J. Millman, N. Mayorov, A. R. J. Nelson, E. Jones, R. Kern, E. Larson, C. J. Carey, I. Polat, Y. Feng, E. W. Moore, J. VanderPlas, D. Laxalde, J. Perktold, R. Cimrman, I. Henriksen, E. A. Quintero, C. R. Harris, A. M. Archibald, A. H. Ribeiro, F. Pedregosa, P. van Mulbregt, and SciPy 1.0 Contributors, Scipy 1.0: Fundamental algorithms for scientific computing in python, *Nat. Methods* **17**, 261 (2020).

[98] L. Amerio and G. Prouse, *Almost-Periodic Functions and Functionals* (Springer New York, NY, 1971).

[99] A. Meurer, C. P. Smith, M. Paprocki, O. Čertík, S. B. Kirpichev, M. Rocklin, A. Kumar, S. Ivanov, J. K. Moore, S. Singh, T. Rathnayake, S. Vig, B. E. Granger, R. P. Muller, F. Bonazzi, H. Gupta, S. Vats, F. Johansson, F. Pedregosa, M. J. Curry, A. R. Terrel, v. Roudka, A. Saboo, I. Fernando, S. Kulal, R. Cimrman, and A. Scopatz, Sympy: symbolic computing in python, *PeerJ Computer Science* **3**, e103 (2017).

[100] N. Hatano and M. Suzuki, Finding exponential product formulas of higher orders, in *Quantum annealing and other optimization methods*, edited by A. K. Das and B. Chakrabarti (Springer, 2005) pp. 37–68.

[101] T. Barthel and Y. Zhang, Optimized lie–trotter–suzuki decompositions for two and three non-commuting terms, *Ann. Phys.* **418**, 168165 (2020).

[102] W. J. Hehre, R. F. Stewart, and J. A. Pople, Self-consistent molecular-orbital methods. I. Use of Gaussian expansions of Slater-type atomic orbitals, *J. Chem. Phys.* **51**, 2657 (1969).

[103] A. Peruzzo, J. McClean, P. Shadbolt, M.-H. Yung, X.-Q. Zhou, P. J. Love, A. Aspuru-Guzik, and J. L.

O'Brien, A variational eigenvalue solver on a photonic quantum processor, *Nat. Commun.* **5**, 4213 (2014).

[104] C. G. Broyden, The convergence of a class of double-rank minimization algorithms: 2. The new algorithm, *IMA J. Appl. Math.* **6**, 222 (1970).

[105] R. Fletcher, A new approach to variable metric algorithms, *Comput. J.* **13**, 317 (1970).

[106] D. Goldfarb, A family of variable-metric methods derived by variational means, *Math. Comp.* **24**, 23 (1970).

[107] D. F. Shanno, Conditioning of quasi-Newton methods for function minimization, *Math. Comp.* **24**, 647 (1970).

[108] N. H. Stair and F. A. Evangelista, QForte: An efficient state-vector emulator and quantum algorithms library for molecular electronic structure, *J. Chem. Theory Comput.* **18**, 1555 (2022).

[109] D. G. A. Smith, L. A. Burns, A. C. Simmonett, R. M. Parrish, M. C. Schieber, R. Galvelis, P. Kraus, H. Kruse, R. D. Remigio, A. Alenaizan, A. M. James, S. Lehtola, J. P. Misiewicz, M. Scheurer, R. A. Shaw, J. B. Schriber, Y. Xie, Z. L. Glick, D. A. Sirianni, J. S. O'Brien, J. M. Waldrop, A. Kumar, E. G. Hohenstein, B. P. Pritchard, B. R. Brooks, H. F. Schaefer III, A. Y. Sokolov, K. Patkowski, A. E. DePrince III, U. Bozkaya, R. A. King, F. A. Evangelista, J. M. Turney, T. D. Crawford, and C. D. Sherrill, Psi4 1.4: Open-source software for high-throughput quantum chemistry, *J. Chem. Phys.* **152**, 184108 (2020).

[110] I. W. Bulik, T. M. Henderson, and G. E. Scuseria, *J. Chem. Theory Comput.* **11**, 3171 (2015).

[111] K. Mitarai, M. Negoro, M. Kitagawa, and K. Fujii, Quantum circuit learning, *Phys. Rev. A* **98**, 032309 (2018).

[112] M. Schuld, V. Bergholm, C. Gogolin, J. Izaac, and N. Killoran, Evaluating analytic gradients on quantum hardware, *Phys. Rev. A* **99**, 032331 (2019).

[113] J. S. Kottmann, A. Anand, and A. Aspuru-Guzik, A feasible approach for automatically differentiable unitary coupled-cluster on quantum computers, *Chem. Sci.* **12**, 3497 (2021).

[114] A. F. Izmaylov, R. A. Lang, and T.-C. Yen, Analytic gradients in variational quantum algorithms: Algebraic extensions of the parameter-shift rule to general unitary transformations, *Phys. Rev. A* **104**, 062443 (2021).

**Supplemental Material:
Spin-Adapted Fermionic Unitaries:
From Lie Algebras to Compact Quantum Circuits**

Ilias Magoulas* and Francesco A. Evangelista

*Department of Chemistry and Cherry Emerson Center for Scientific Computation,
Emory University, Atlanta, Georgia 30322, USA*

*Corresponding author; e-mail: ilias.magoulas@emory.edu.

S1. COMPUTATIONAL DETAILS

All symbolic manipulations were performed with SymPy. For each spin-adapted unitary $\exp(\theta \sum_i A_i)$, we first computed the Lie closure of the set of spinorbital operators $\{A_i\}$. This was accomplished by iteratively closing the set under commutation. Specifically, for every pair (X, Y) drawn from the current list of basis elements, we computed the commutator $[X, Y]$, simplified the resulting expression, and added it to the basis if it was nonzero and linearly independent from the existing elements. The newly added operators were then commuted with both the original generators and with the other new elements until no further linearly independent operators emerged. To enable the efficient circuit implementation of the corresponding unitaries, we took linear combinations of the basis elements so that they could take the form of an anti-Hermitian excitation operator A_i multiplied, at most, by a linear combination of two particle-hole-conjugate number-operator strings N_i . The final ordered basis $\{E_i\}$ of the dynamical Lie algebra was then constructed by grouping the basis elements into commuting sets.

Subsequently, we computed symbolic expressions for $[E_i, E_j]$, $[[E_i, E_j], E_j]$, and $E_j[E_i, E_j]E_j$, and used these to evaluate in closed form the unitary transformations appearing in the Wei–Norman procedure. Finally, we symbolically built the Wei–Norman system of coupled ordinary differential equations in matrix form,

$$\mathbf{A}(\theta, \boldsymbol{\alpha})\boldsymbol{\alpha}'(\theta) = \mathbf{d}(\theta), \quad (\text{S1})$$

where \mathbf{A} is the Wei–Norman coefficient matrix, $\boldsymbol{\alpha}$ is the vector of θ -dependent parameters, $\boldsymbol{\alpha}' = \frac{d\boldsymbol{\alpha}}{d\theta}$, and \mathbf{d} is the vector containing the coefficients multiplying the basis elements of the dynamical Lie algebra in the target spin-adapted unitary.

The symbolic expressions for \mathbf{A} and \mathbf{d} were converted to numerical callables. The numerical integration of the Wei–Norman system of equations was performed using the initial-value-problem solver from SciPy. The interval of integration was typically set to $[0, 10]$ and the solution was sampled on 2001 uniformly spaced points. For the smallest dynamical Lie algebra considered in this work, we also considered the extended range $[-100, 100]$ with 20001 sampled points. We used the DOP853 integration method, with relative and absolute tolerances set to $\text{rtol} = 10^{-9}$ and $\text{atol} = 10^{-12}$, respectively.

For the largest dynamical Lie algebra considered in our work, a fully symbolic construction of the

Wei–Norman system of equations was computationally too demanding. As described in the main text, in this case the θ -dependent parameters were obtained by minimizing the Frobenius norm of the difference between the target unitary and its Wei–Norman decomposition, both represented as matrices in the minimal Fock space of 8 spinorbitals. For each $\theta \in [0, 10]$, sampled on 2001 uniformly spaced points, the minimization was performed with the BFGS method as implemented in SciPy. We employed the 3-point numerical derivatives, the gradient tolerance was set to $\text{gtol} = 10^{-6}$, and the maximum number of iterations was set to 2000. To verify the robustness of this strategy, for the smaller Lie algebras we compared the optimized parameters against those obtained from the numerical integration of the Wei–Norman system of coupled ordinary differential equations. The maximum deviation in the parameters were found to be $< 10^{-6}$.

S2. PROOF OF CLOSED-FORM SIMILARITY-TRANSFORMATION EXPRESSION

To derive the closed-form expression of the unitary transformation shown in Eq. (21) in the main text, we work as follows. First, we note that a generic element E_j of the dynamical Lie algebras obtained in this work has the form

$$E_j = A_j N_j, \quad (\text{S2})$$

where A_j is an anti-Hermitian two-body fermionic excitation operator,

$$A_j = F_j - F_j^\dagger, \quad (\text{S3})$$

with F_j being a two-body fermionic string, and N_j is a linear combination of two particle–hole-conjugate number-operator strings, satisfying $N_j^2 = N_j$. Note that A_j and N_j share no indices by construction and, thus, they commute, $[A_j, N_j] = 0$. Following our previous work on deriving closed-form fermionic unitary transformations (Ref. [95] in the main text), we examine the various powers of E_j , obtaining

$$\begin{aligned} E_j^2 &= A_j N_j A_j N_j \\ &= A_j^2 N_j^2 \\ &= -(F_j F_j^\dagger + F_j^\dagger F_j) N_j \end{aligned} \quad (\text{S4})$$

and

$$\begin{aligned}
E_j^3 &= A_j^3 N_j^3 \\
&= -A_j N_j \\
&= -E_j,
\end{aligned} \tag{S5}$$

where we used the fact that the fermionic string F_j is nilpotent, $F_j^2 = 0$. As shown in Ref. [95] in the main text, the above closure relation directly leads to

$$[[[E_i, E_j], E_j], E_j] = -[E_i, E_j] - 3E_j[E_i, E_j]E_j. \tag{S6}$$

To prove that the unitary transformation $\exp(\alpha_j E_j)E_i\exp(-\alpha_j E_j)$ proceeds via Eq. (21) in the main text, it suffices to show that $E_j[E_i, E_j]E_j = 0$ for every pair of basis elements E_i and E_j (see Ref. [95] for the details). The above equality holds in the trivial case $[E_i, E_j] = 0$, *i.e.*, when A_i and A_j have no common indices or when $A_i = A_j$. When A_i and A_j share only a subset of their indices, we use the fact that $\{E_i\}$ is a basis of the pertinent dynamical Lie algebra, allowing us to write

$$[E_i, E_j] = c_{ij}^k E_k, \tag{S7}$$

where we use the Einstein summation convention of repeated upper and lower indices. Using Eq. (S7), we arrive at

$$E_j[E_i, E_j]E_j = c_{ij}^k E_j E_k E_j. \tag{S8}$$

Since each A_μ is an anti-Hermitian linear combination of two fermionic strings and N_μ is a linear combination of two particle-hole conjugate number operator strings, each $E_j E_k E_j$ term in Eq. (S8) gives rise to a linear combination of, at most, 64 fermionic strings. Subsequently, we use the fact that all indices of E_j appear in each E_k . Indeed, the number operator component N_k of E_k contains the indices shared between E_i and E_j , while the remaining indices of E_i and E_j form the excitation part of E_k , namely A_k . Because of this structure, equation Eq. (S8) equals 0 due to the nilpotency of elementary annihilation and creation operators, as in each of the fermionic strings appearing in it there will be at least one pair of annihilation/creation operators with the same index. Consequently, we obtain Eq. (21) in the main text.

S3. CLASSIFICATION OF THE LIE ALGEBRA $\text{Lie}(A_{P\uparrow}^{Q\uparrow R\downarrow}, A_{P\uparrow}^{Q\downarrow R\uparrow})$

In this section, we show that the 5-dimensional dynamical Lie algebra $\text{Lie}(A_{P\uparrow P\downarrow}^{Q\uparrow R\downarrow}, A_{P\uparrow P\downarrow}^{Q\downarrow R\uparrow})$ is isomorphic to the Lie algebra direct sum $\mathbb{R}^2 \oplus \mathfrak{so}(3)$ or, equivalently, $\mathbb{R}^2 \oplus \mathfrak{su}(2)$.

As shown in the main text, a convenient basis is $\text{Lie}\left(A_{P\uparrow P\downarrow}^{Q\uparrow R\downarrow}, A_{P\uparrow P\downarrow}^{Q\downarrow R\uparrow}\right) = \text{span}(\{E_i\}_{i=1}^5)$, with $E_1 \equiv A_{P\uparrow P\downarrow}^{Q\uparrow R\downarrow}$, $E_2 \equiv A_{P\uparrow P\downarrow}^{Q\downarrow R\uparrow}$, $E_3 \equiv A_{P\uparrow P\downarrow}^{Q\uparrow R\downarrow}(h_{Q\downarrow R\uparrow} + n_{Q\downarrow R\uparrow})$, $E_4 \equiv A_{P\uparrow P\downarrow}^{Q\downarrow R\uparrow}(h_{Q\uparrow R\downarrow} + n_{Q\uparrow R\downarrow})$, and $E_5 \equiv A_{Q\uparrow R\downarrow}^{Q\downarrow R\uparrow}(h_{P\uparrow P\downarrow} - n_{P\uparrow P\downarrow})$. The commutation matrix \mathbf{C} , whose elements are defined as $C_{ij} = [E_i, E_j]$, is

$$\mathbf{C} = \begin{pmatrix} 0 & E_5 & 0 & E_5 & -E_4 \\ -E_5 & 0 & -E_5 & 0 & E_3 \\ 0 & E_5 & 0 & E_5 & -E_4 \\ -E_5 & 0 & -E_5 & 0 & E_3 \\ E_4 & -E_3 & E_4 & -E_3 & 0 \end{pmatrix}. \quad (\text{S9})$$

A quick inspection of Eq. (S9) reveals that E_3 , E_4 , and E_5 satisfy commutation relations of the form $[E_i, E_j] = \varepsilon_{ij}^k E_k$, with ε_{ij}^k denoting the Levi-Civita symbol. Thus, the set $\{A_{P\uparrow P\downarrow}^{Q\uparrow R\downarrow}(h_{Q\downarrow R\uparrow} + n_{Q\downarrow R\uparrow}), A_{P\uparrow P\downarrow}^{Q\downarrow R\uparrow}(h_{Q\uparrow R\downarrow} + n_{Q\uparrow R\downarrow}), A_{Q\uparrow R\downarrow}^{Q\downarrow R\uparrow}(h_{P\uparrow P\downarrow} - n_{P\uparrow P\downarrow})\}$ generates a Lie subalgebra isomorphic to $\mathfrak{so}(3) \cong \mathfrak{su}(2)$.

Subsequently, we change the basis by replacing the elements E_1 and E_2 by $\tilde{E}_1 = E_3 - E_1$ and $\tilde{E}_2 = E_4 - E_2$, respectively. In doing so, we obtain

$$\begin{aligned} [\tilde{E}_1, \tilde{E}_2] &= [E_3 - E_1, E_4 - E_2] \\ &= [E_3, E_4] - [E_3, E_2] - [E_1, E_4] + [E_1, E_2] \\ &= 0, \end{aligned} \quad (\text{S10})$$

where we used Eq. (S9). Thus, the set $\{A_{P\uparrow P\downarrow}^{Q\uparrow R\downarrow}(h_{Q\downarrow R\uparrow} + n_{Q\downarrow R\uparrow}) - A_{P\uparrow P\downarrow}^{Q\uparrow R\downarrow}, A_{P\uparrow P\downarrow}^{Q\downarrow R\uparrow}(h_{Q\uparrow R\downarrow} + n_{Q\uparrow R\downarrow}) - A_{P\uparrow P\downarrow}^{Q\downarrow R\uparrow}\}$ spans an abelian 2-dimensional Lie algebra and, therefore, it is isomorphic to \mathbb{R}^2 . Furthermore, from Eq. (S9) we immediately observe that $[\tilde{E}_i, E_j] = 0$ for $i = 1, 2$ and $j = 3, 4, 5$. As a result, we obtain $\text{Lie}(A_{P\uparrow P\downarrow}^{Q\uparrow R\downarrow}, A_{P\uparrow P\downarrow}^{Q\downarrow R\uparrow}) \cong \mathbb{R}^2 \oplus \mathfrak{so}(3) \cong \mathbb{R}^2 \oplus \mathfrak{su}(2)$.

S4. EFFECT OF PERMUTATIONS IN THE WEI–NORMAN DECOMPOSITIONS OF $\exp(A_{PP}^{QR})$

As an illustration of the effect of permuting the exponentials appearing in the Wei–Norman decomposition of spin-adapted unitaries, we computed all 120 permutations of the five exponentials defining the Wei–Norman decomposition of $\exp(A_{PP}^{QR})$.

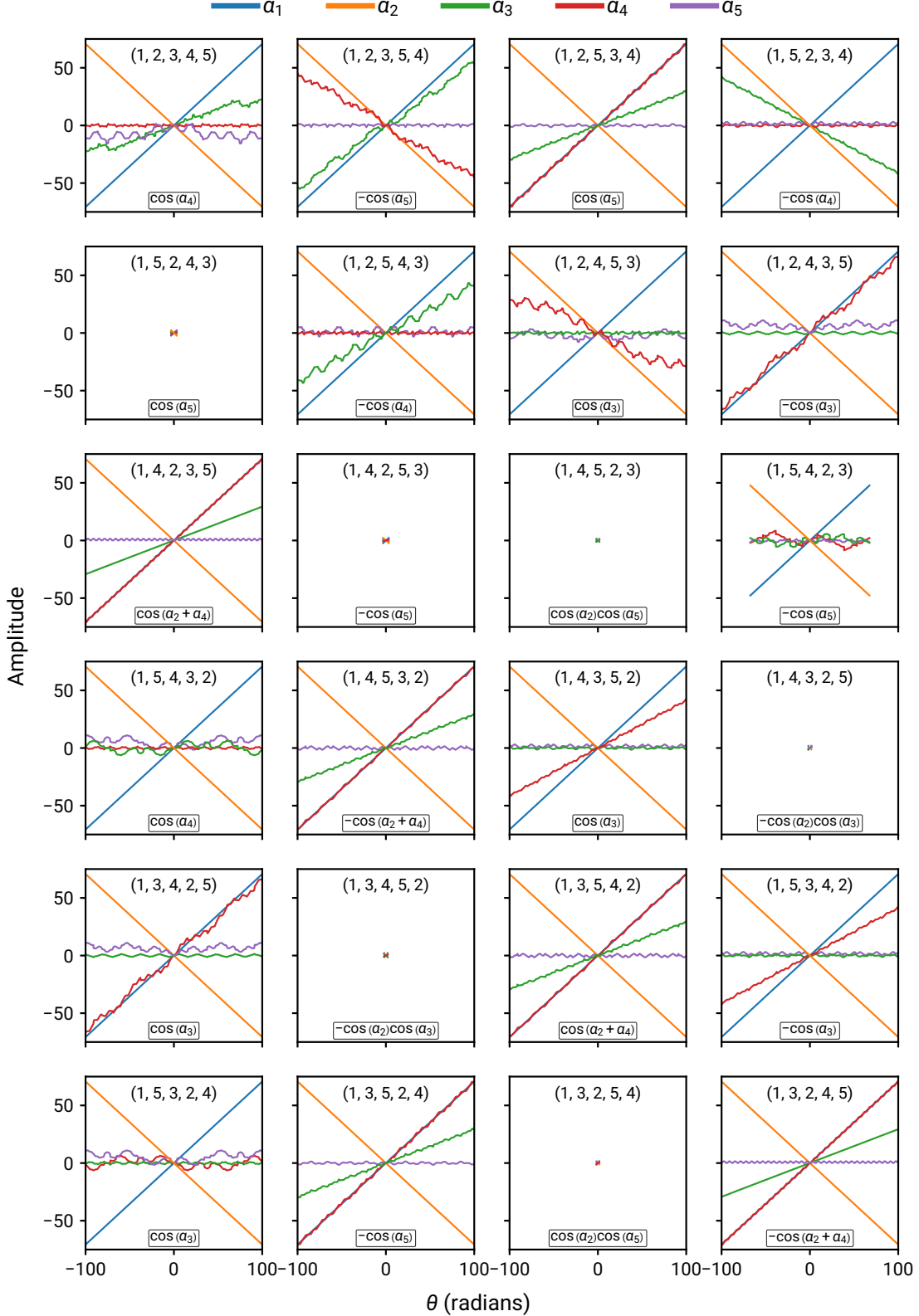
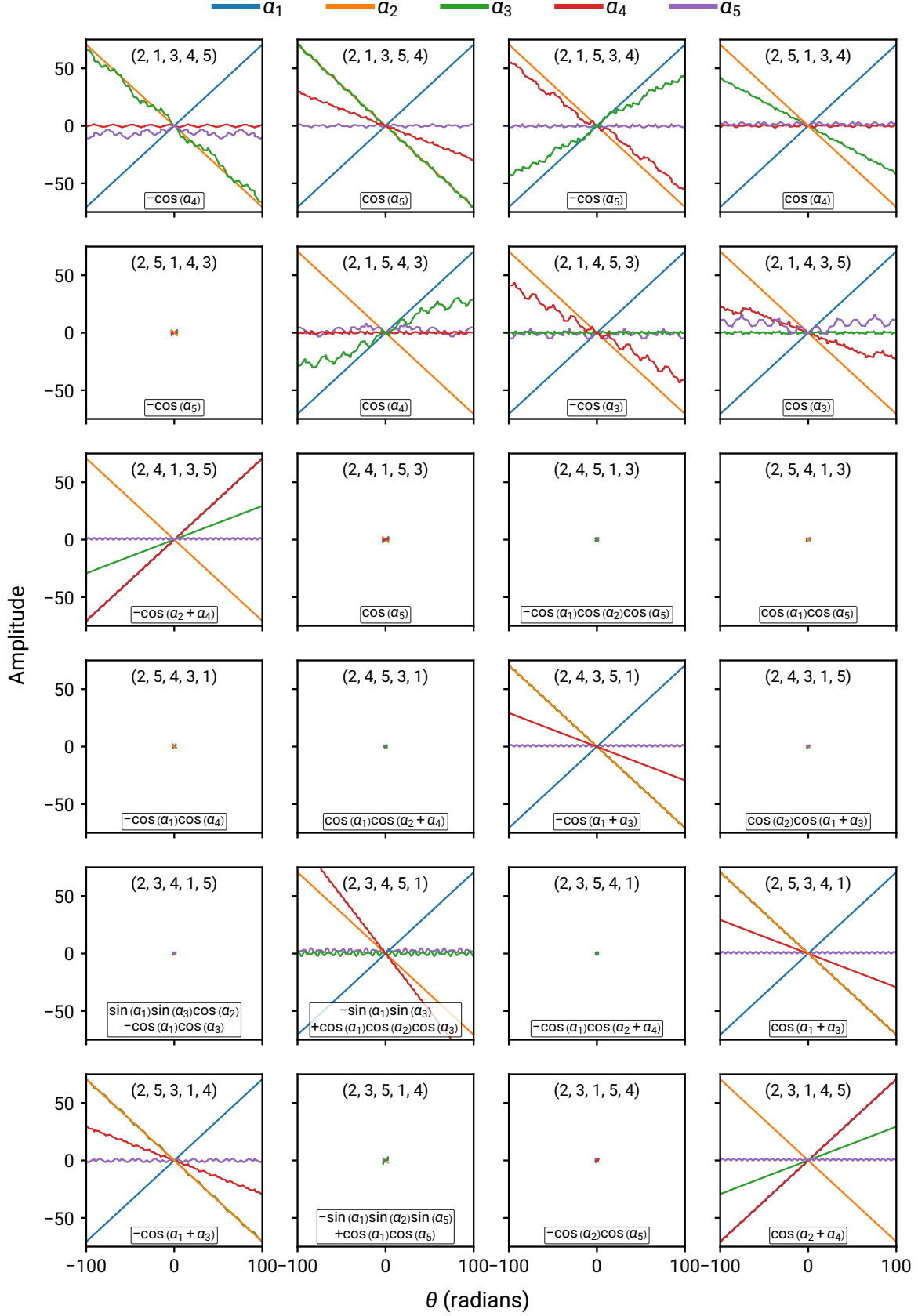
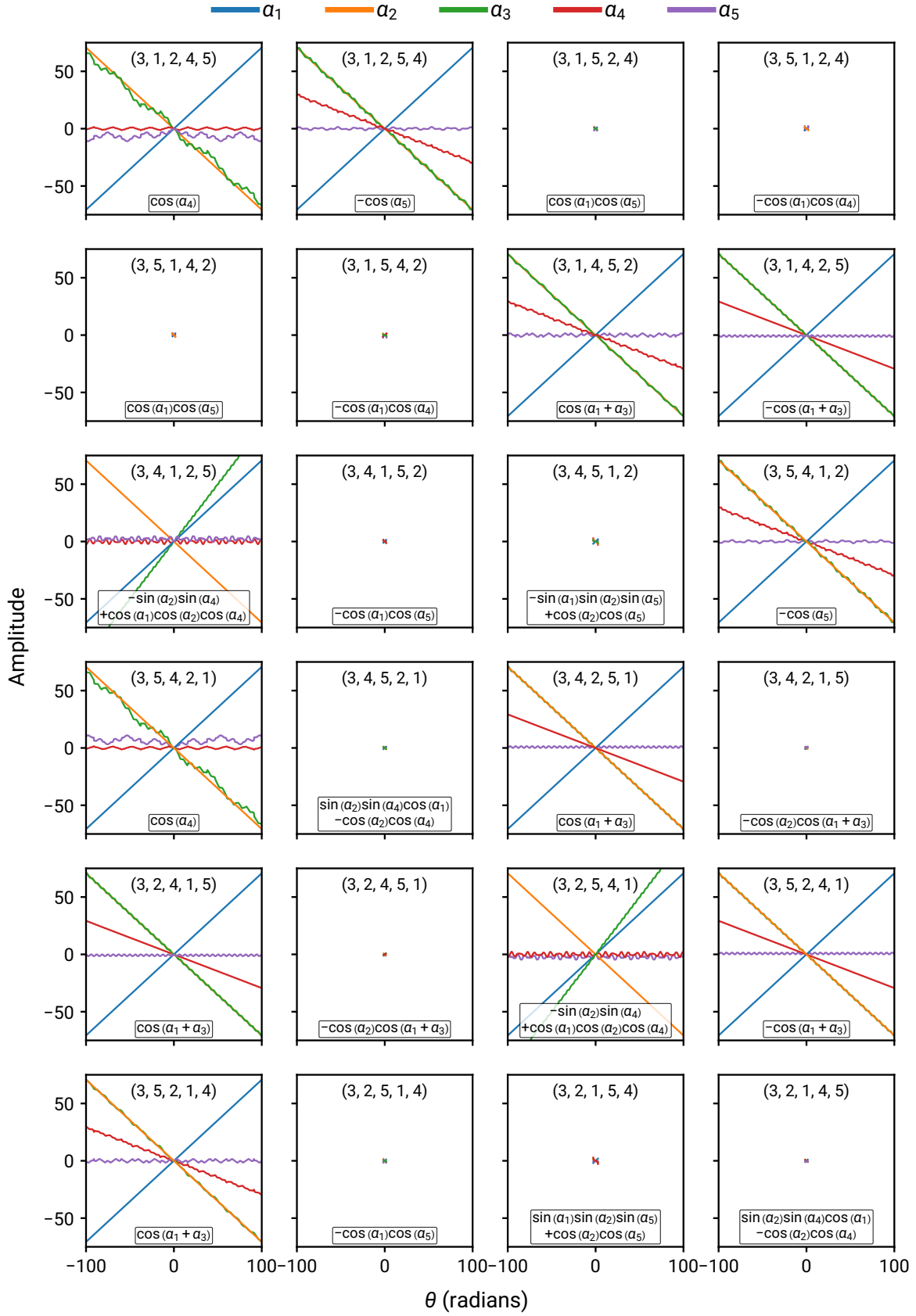
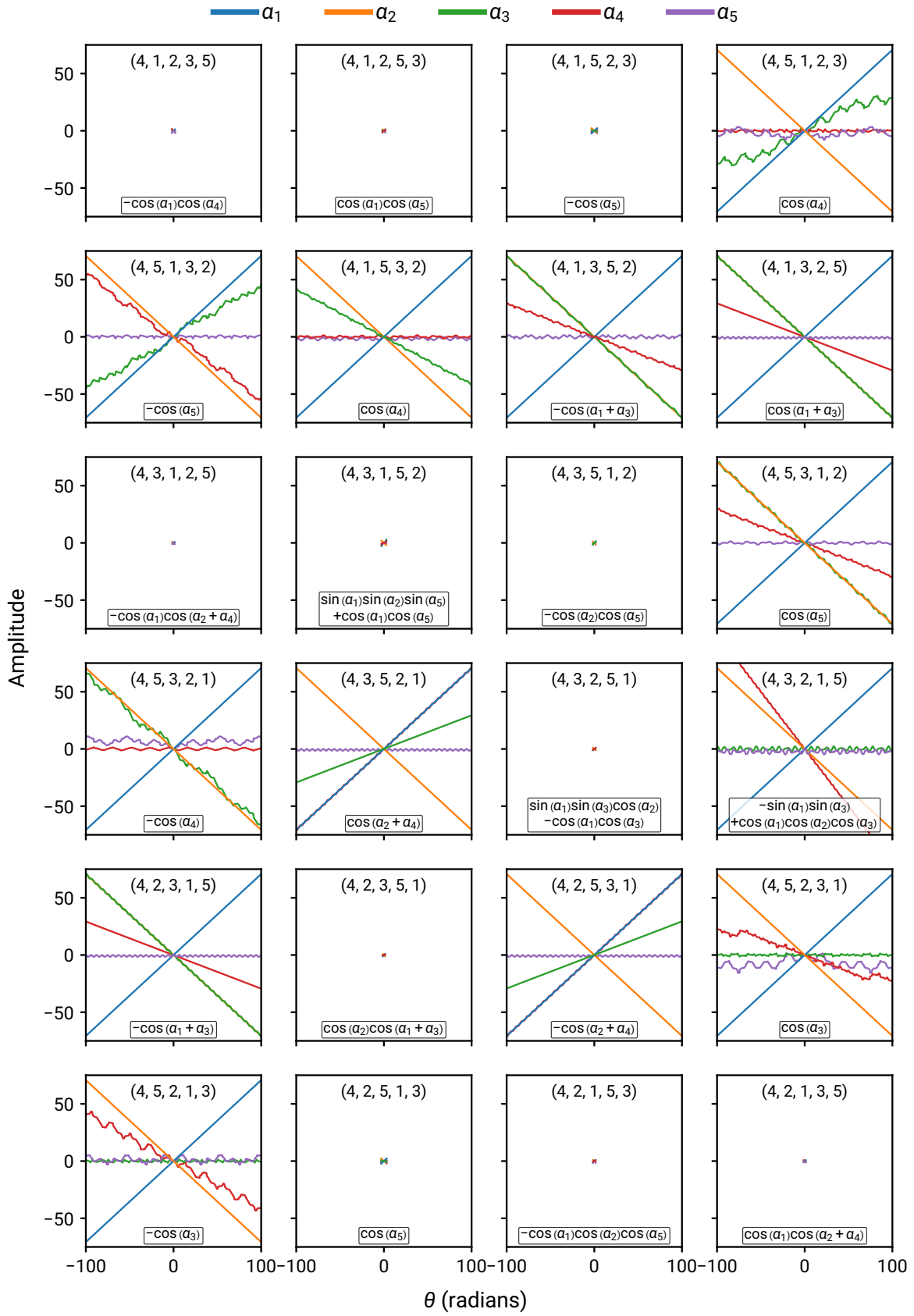
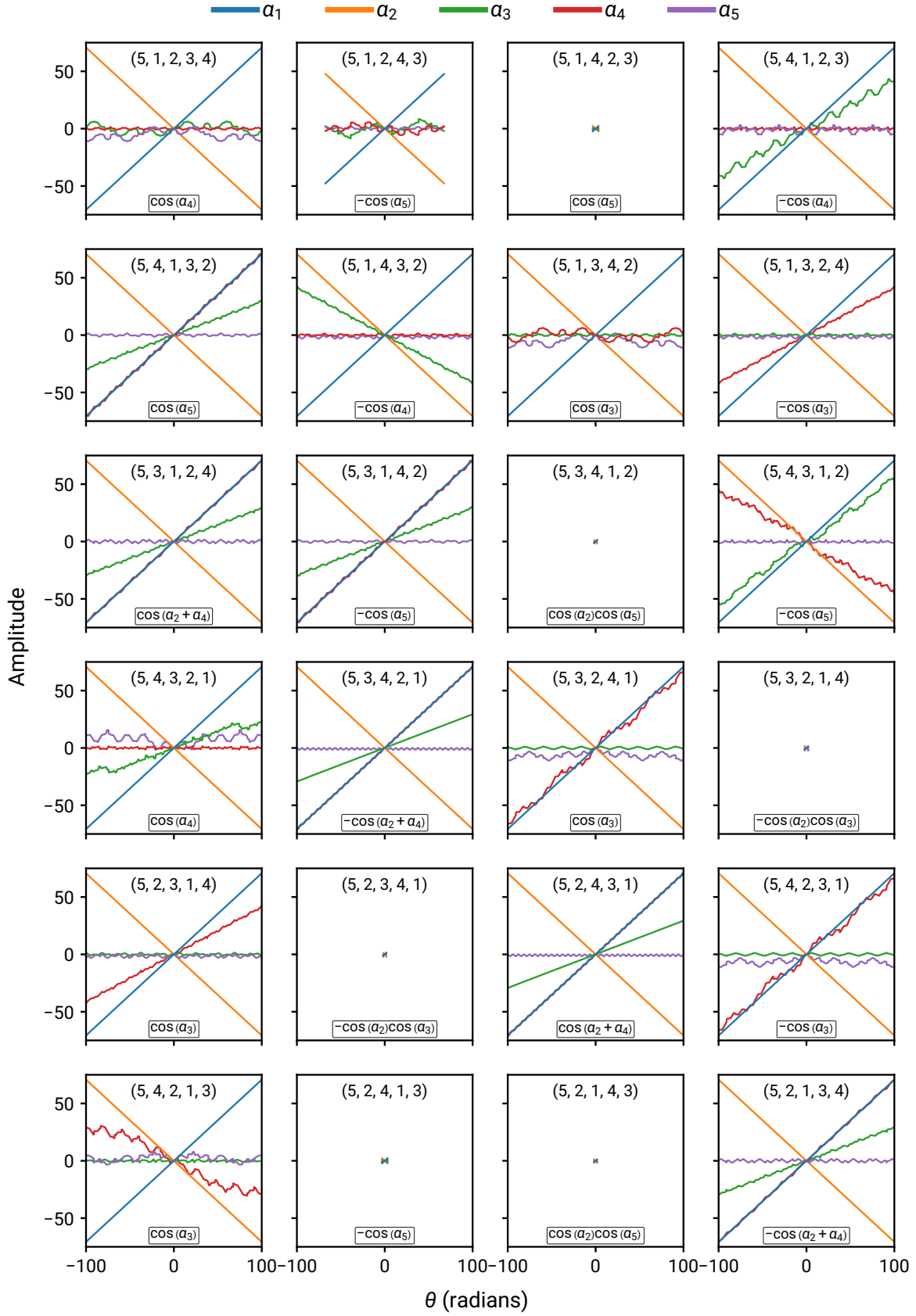


FIG. S1. Parameters defining the Wei–Norman decompositions of $\exp(\theta A_{PP}^{QR})$ [Eq. (18)], with $\exp(\alpha_1 E_1)$ in the first position. In each panel, the permutation is given in parentheses, and the determinant of the Wei–Norman coefficient matrix is shown in the rounded box.

FIG. S2. Same as Fig. S1, but with $\exp(a_2 E_2)$ in the first position.

FIG. S3. Same as Fig. S1, but with $\exp(\alpha_3 E_3)$ in the first position.

FIG. S4. Same as Fig. S1, but with $\exp(\alpha_4 E_4)$ in the first position.

FIG. S5. Same as Fig. S1, but with $\exp(\alpha_5 E_5)$ in the first position.

S5. DYNAMICAL LIE ALGEBRAS OF ${}^{[0]}A_{PQ}^{RS}$ AND ${}^{[1]}A_{PQ}^{RS}$

TABLE S1: Basis elements spanning the dynamical Lie algebra of ${}^{[0]}A_{PQ}^{RS}$, $\mathfrak{g} \equiv \text{Lie}\{A_{P\uparrow Q\downarrow}^{R\uparrow S\downarrow}, A_{P\downarrow Q\uparrow}^{R\downarrow S\uparrow}, A_{P\uparrow Q\downarrow}^{R\downarrow S\uparrow}, A_{P\downarrow Q\uparrow}^{R\uparrow S\downarrow}\}$.^a

Basis element	Wei–Norman coefficient
$A_{P\uparrow Q\downarrow}^{R\uparrow S\downarrow}$	$\frac{\theta}{2}$
$A_{P\uparrow Q\downarrow}^{R\uparrow S\downarrow} (h_{P\downarrow Q\uparrow} + n_{P\downarrow Q\uparrow})$	$c_1(\theta)$
$A_{P\uparrow Q\downarrow}^{R\uparrow S\downarrow} (h_{R\downarrow S\uparrow} + n_{R\downarrow S\uparrow})$	$c_1(\theta)$
$A_{P\uparrow Q\downarrow}^{R\uparrow S\downarrow} (h_{P\downarrow Q\uparrow R\downarrow S\uparrow} + n_{P\downarrow Q\uparrow R\downarrow S\uparrow})$	$c_2(\theta)$
$A_{P\uparrow Q\downarrow}^{R\uparrow S\downarrow} (n_{R\downarrow S\uparrow} h_{P\downarrow Q\uparrow} + n_{P\downarrow Q\uparrow} h_{R\downarrow S\uparrow})$	$c_3(\theta)$
$A_{P\downarrow Q\uparrow}^{R\downarrow S\uparrow}$	$\frac{\theta}{2}$
$A_{P\downarrow Q\uparrow}^{R\downarrow S\uparrow} (h_{P\uparrow Q\downarrow} + n_{P\uparrow Q\downarrow})$	$c_1(\theta)$
$A_{P\downarrow Q\uparrow}^{R\downarrow S\uparrow} (h_{R\uparrow S\downarrow} + n_{R\uparrow S\downarrow})$	$c_1(\theta)$
$A_{P\downarrow Q\uparrow}^{R\downarrow S\uparrow} (h_{P\uparrow Q\downarrow R\uparrow S\downarrow} + n_{P\uparrow Q\downarrow R\uparrow S\downarrow})$	$c_2(\theta)$
$A_{P\downarrow Q\uparrow}^{R\downarrow S\uparrow} (n_{R\uparrow S\downarrow} h_{P\downarrow Q\uparrow} + n_{P\downarrow Q\uparrow} h_{R\uparrow S\downarrow})$	$c_3(\theta)$
$A_{P\uparrow Q\downarrow}^{R\downarrow S\uparrow}$	$-\frac{\theta}{2}$
$A_{P\uparrow Q\downarrow}^{R\downarrow S\uparrow} (h_{P\downarrow Q\uparrow} + n_{P\downarrow Q\uparrow})$	$c_4(\theta)$
$A_{P\uparrow Q\downarrow}^{R\downarrow S\uparrow} (h_{R\uparrow S\downarrow} + n_{R\uparrow S\downarrow})$	$c_4(\theta)$
$A_{P\uparrow Q\downarrow}^{R\downarrow S\uparrow} (h_{P\downarrow Q\uparrow R\uparrow S\downarrow} + n_{P\downarrow Q\uparrow R\uparrow S\downarrow})$	$c_5(\theta)$
$A_{P\uparrow Q\downarrow}^{R\downarrow S\uparrow} (n_{R\uparrow S\downarrow} h_{P\downarrow Q\uparrow} + n_{P\downarrow Q\uparrow} h_{R\uparrow S\downarrow})$	$c_6(\theta)$
$A_{P\downarrow Q\uparrow}^{R\uparrow S\downarrow}$	$-\frac{\theta}{2}$
$A_{P\downarrow Q\uparrow}^{R\uparrow S\downarrow} (h_{P\uparrow Q\downarrow} + n_{P\uparrow Q\downarrow})$	$c_4(\theta)$
$A_{P\downarrow Q\uparrow}^{R\uparrow S\downarrow} (h_{R\downarrow S\uparrow} + n_{R\downarrow S\uparrow})$	$c_4(\theta)$
$A_{P\downarrow Q\uparrow}^{R\uparrow S\downarrow} (h_{P\uparrow Q\downarrow R\downarrow S\uparrow} + n_{P\uparrow Q\downarrow R\downarrow S\uparrow})$	$c_5(\theta)$
$A_{P\downarrow Q\uparrow}^{R\uparrow S\downarrow} (n_{R\downarrow S\uparrow} h_{P\uparrow Q\downarrow} + n_{P\uparrow Q\downarrow} h_{R\downarrow S\uparrow})$	$c_6(\theta)$
$A_{P\uparrow Q\downarrow}^{P\downarrow Q\uparrow} (h_{R\uparrow S\downarrow} - n_{R\uparrow S\downarrow})$	$c_7(\theta)$
$A_{P\uparrow Q\downarrow}^{P\downarrow Q\uparrow} (h_{R\downarrow S\uparrow} - n_{R\downarrow S\uparrow})$	$-c_7(\theta)$
$A_{P\uparrow Q\downarrow}^{P\downarrow Q\uparrow} (n_{R\downarrow S\uparrow} h_{R\uparrow S\downarrow} - n_{R\uparrow S\downarrow} h_{R\downarrow S\uparrow})$	$c_8(\theta)$
$A_{P\uparrow Q\downarrow}^{P\downarrow Q\uparrow} (h_{R\uparrow R\downarrow S\uparrow S\downarrow} - n_{R\uparrow R\downarrow S\uparrow S\downarrow})$	0
$A_{R\uparrow S\downarrow}^{R\downarrow S\uparrow} (h_{P\uparrow Q\downarrow} - n_{P\uparrow Q\downarrow})$	$c_7(\theta)$
$A_{R\uparrow S\downarrow}^{R\downarrow S\uparrow} (h_{P\downarrow Q\uparrow} - n_{P\downarrow Q\uparrow})$	$-c_7(\theta)$
$A_{R\uparrow S\downarrow}^{R\downarrow S\uparrow} (n_{P\downarrow Q\uparrow} h_{P\uparrow Q\downarrow} - n_{P\uparrow Q\downarrow} h_{P\downarrow Q\uparrow})$	$c_8(\theta)$
$A_{R\uparrow S\downarrow}^{R\downarrow S\uparrow} (h_{P\uparrow P\downarrow Q\uparrow Q\downarrow} - n_{P\uparrow P\downarrow Q\uparrow Q\downarrow})$	0

^aThin partial horizontal rules separate basis elements that differ in the anti-Hermitian excitation part. Thick horizontal rules separate mutually commuting sets.

TABLE S2: Basis elements spanning the dynamical Lie algebra of ${}^{[1]}A_{PQ}^{RS}$, $\mathfrak{g} \equiv \text{Lie}\{A_{P\uparrow Q\uparrow}^{R\uparrow S\uparrow}, A_{P\downarrow Q\downarrow}^{R\downarrow S\downarrow}, A_{P\uparrow Q\downarrow}^{R\uparrow S\downarrow}, A_{P\downarrow Q\uparrow}^{R\downarrow S\uparrow}, A_{P\uparrow Q\downarrow}^{R\downarrow S\downarrow}\}.$ ^a

Basis element	Wei–Norman coefficient
$A_{P\uparrow Q\uparrow}^{R\uparrow S\uparrow}$	$\frac{\theta}{\sqrt{3}}$
$A_{P\uparrow Q\uparrow}^{R\uparrow S\uparrow} (n_{S\downarrow}h_{Q\downarrow} + n_{Q\downarrow}h_{S\downarrow})$	$c_1(\theta)$
$A_{P\uparrow Q\uparrow}^{R\uparrow S\uparrow} (n_{R\downarrow}h_{P\downarrow} + n_{P\downarrow}h_{R\downarrow})$	$c_1(\theta)$
$A_{P\uparrow Q\uparrow}^{R\uparrow S\uparrow} (n_{R\downarrow}h_{Q\downarrow} + n_{Q\downarrow}h_{R\downarrow})$	$c_1(\theta)$
$A_{P\uparrow Q\uparrow}^{R\uparrow S\uparrow} (n_{S\downarrow}h_{P\downarrow} + n_{P\downarrow}h_{S\downarrow})$	$c_1(\theta)$
$A_{P\uparrow Q\uparrow}^{R\uparrow S\uparrow} (n_{R\downarrow}h_{S\downarrow}h_{Q\downarrow} + n_{Q\downarrow}h_{R\downarrow}h_{S\downarrow})$	$c_2(\theta)$
$A_{P\uparrow Q\uparrow}^{R\uparrow S\uparrow} (n_{S\downarrow}h_{P\downarrow}h_{Q\downarrow} + n_{P\downarrow}h_{Q\downarrow}h_{S\downarrow})$	$c_2(\theta)$
$A_{P\uparrow Q\uparrow}^{R\uparrow S\uparrow} (n_{R\downarrow}h_{P\downarrow}h_{Q\downarrow} + n_{P\downarrow}h_{Q\downarrow}h_{R\downarrow})$	$c_2(\theta)$
$A_{P\uparrow Q\uparrow}^{R\uparrow S\uparrow} (n_{R\downarrow}h_{S\downarrow}h_{P\downarrow} + n_{P\downarrow}h_{R\downarrow}h_{S\downarrow})$	$c_2(\theta)$
$A_{P\uparrow Q\uparrow}^{R\uparrow S\uparrow} (n_{Q\downarrow}h_{R\downarrow}h_{P\downarrow}h_{S\downarrow} + n_{P\downarrow}h_{S\downarrow}h_{Q\downarrow}h_{R\downarrow})$	$c_4(\theta)$
$A_{P\uparrow Q\uparrow}^{R\uparrow S\uparrow} (n_{Q\downarrow}h_{S\downarrow}h_{P\downarrow}h_{R\downarrow} + n_{P\downarrow}h_{R\downarrow}h_{Q\downarrow}h_{S\downarrow})$	$c_4(\theta)$
$A_{P\downarrow Q\downarrow}^{R\downarrow S\downarrow}$	$\frac{\theta}{\sqrt{3}}$
$A_{P\downarrow Q\downarrow}^{R\downarrow S\downarrow} (n_{R\uparrow}h_{P\uparrow} + n_{P\uparrow}h_{R\uparrow})$	$c_1(\theta)$
$A_{P\downarrow Q\downarrow}^{R\downarrow S\downarrow} (n_{S\uparrow}h_{Q\uparrow} + n_{Q\uparrow}h_{S\uparrow})$	$c_1(\theta)$
$A_{P\downarrow Q\downarrow}^{R\downarrow S\downarrow} (n_{S\uparrow}h_{P\uparrow} + n_{P\uparrow}h_{S\uparrow})$	$c_1(\theta)$
$A_{P\downarrow Q\downarrow}^{R\downarrow S\downarrow} (n_{R\uparrow}h_{Q\uparrow} + n_{Q\uparrow}h_{R\uparrow})$	$c_1(\theta)$
$A_{P\downarrow Q\downarrow}^{R\downarrow S\downarrow} (n_{R\uparrow}h_{S\uparrow}h_{P\uparrow} + n_{P\uparrow}h_{R\uparrow}h_{S\uparrow})$	$c_2(\theta)$
$A_{P\downarrow Q\downarrow}^{R\downarrow S\downarrow} (n_{R\uparrow}h_{P\uparrow}h_{Q\uparrow} + n_{P\uparrow}h_{Q\uparrow}h_{R\uparrow})$	$c_2(\theta)$
$A_{P\downarrow Q\downarrow}^{R\downarrow S\downarrow} (n_{S\uparrow}h_{P\uparrow}h_{Q\uparrow} + n_{P\uparrow}h_{Q\uparrow}h_{S\uparrow})$	$c_2(\theta)$
$A_{P\downarrow Q\downarrow}^{R\downarrow S\downarrow} (n_{R\uparrow}h_{S\uparrow}h_{Q\uparrow} + n_{Q\uparrow}h_{R\uparrow}h_{S\uparrow})$	$c_2(\theta)$
$A_{P\downarrow Q\downarrow}^{R\downarrow S\downarrow} (n_{R\uparrow}h_{S\uparrow}h_{P\uparrow}h_{Q\uparrow} + n_{P\uparrow}h_{Q\uparrow}h_{R\uparrow}h_{S\uparrow})$	$c_3(\theta)$
$A_{P\downarrow Q\downarrow}^{R\downarrow S\downarrow} (n_{Q\uparrow}h_{R\uparrow}h_{P\uparrow}h_{S\uparrow} + n_{P\uparrow}h_{S\uparrow}h_{Q\uparrow}h_{R\uparrow})$	$c_4(\theta)$
$A_{P\downarrow Q\downarrow}^{R\downarrow S\downarrow} (n_{Q\uparrow}h_{S\uparrow}h_{P\uparrow}h_{R\uparrow} + n_{P\uparrow}h_{R\uparrow}h_{Q\uparrow}h_{S\uparrow})$	$c_4(\theta)$
$A_{P\uparrow Q\downarrow}^{R\uparrow S\downarrow}$	$\frac{\theta}{2\sqrt{3}}$
$A_{P\uparrow Q\downarrow}^{R\uparrow S\downarrow} (n_{S\uparrow}h_{Q\uparrow} + n_{Q\uparrow}h_{S\uparrow})$	$c_5(\theta)$
$A_{P\uparrow Q\downarrow}^{R\uparrow S\downarrow} (n_{R\downarrow}h_{P\downarrow} + n_{P\downarrow}h_{R\downarrow})$	$c_5(\theta)$
$A_{P\uparrow Q\downarrow}^{R\uparrow S\downarrow} (h_{R\downarrow}h_{S\uparrow} + n_{R\downarrow}h_{S\uparrow})$	$c_5(\theta)$
$A_{P\uparrow Q\downarrow}^{R\uparrow S\downarrow} (h_{P\downarrow}h_{Q\uparrow} + n_{P\downarrow}h_{Q\uparrow})$	$c_5(\theta)$
$A_{P\uparrow Q\downarrow}^{R\uparrow S\downarrow} (n_{R\downarrow}h_{S\uparrow}h_{Q\uparrow} + n_{Q\uparrow}h_{R\downarrow}h_{S\uparrow})$	$c_6(\theta)$
$A_{P\uparrow Q\downarrow}^{R\uparrow S\downarrow} (n_{S\uparrow}h_{P\downarrow}h_{Q\uparrow} + n_{P\downarrow}h_{Q\uparrow}h_{S\uparrow})$	$c_6(\theta)$
$A_{P\uparrow Q\downarrow}^{R\uparrow S\downarrow} (n_{R\downarrow}h_{S\uparrow}h_{P\downarrow} + n_{P\downarrow}h_{R\downarrow}h_{S\uparrow})$	$c_6(\theta)$
$A_{P\uparrow Q\downarrow}^{R\uparrow S\downarrow} (n_{R\downarrow}h_{P\downarrow}h_{Q\uparrow} + n_{P\downarrow}h_{Q\uparrow}h_{R\downarrow})$	$c_6(\theta)$

Continued on next page.

TABLE S2: Continued from previous page

Basis element	Wei–Norman coefficient
$A_{P\uparrow Q\downarrow}^{R\uparrow S\downarrow} (n_{R\downarrow S\uparrow} h_{P\downarrow Q\uparrow} + n_{P\downarrow Q\uparrow} h_{R\downarrow S\uparrow})$	$c_7(\theta)$
$A_{P\uparrow Q\downarrow}^{R\uparrow S\downarrow} (h_{P\downarrow Q\uparrow R\downarrow S\uparrow} + n_{P\downarrow Q\uparrow R\downarrow S\uparrow})$	$c_8(\theta)$
$A_{P\uparrow Q\downarrow}^{R\uparrow S\downarrow} (n_{Q\uparrow R\downarrow} h_{P\downarrow S\uparrow} + n_{P\downarrow S\uparrow} h_{Q\uparrow R\downarrow})$	$c_8(\theta)$
$A_{P\downarrow Q\uparrow}^{R\downarrow S\uparrow}$	$\frac{\theta}{2\sqrt{3}}$
$A_{P\downarrow Q\uparrow}^{R\downarrow S\uparrow} (n_{R\uparrow} h_{P\uparrow} + n_{P\uparrow} h_{R\uparrow})$	$c_5(\theta)$
$A_{P\downarrow Q\uparrow}^{R\downarrow S\uparrow} (n_{S\downarrow} h_{Q\downarrow} + n_{Q\downarrow} h_{S\downarrow})$	$c_5(\theta)$
$A_{P\downarrow Q\uparrow}^{R\downarrow S\uparrow} (h_{P\uparrow Q\downarrow} + n_{P\uparrow Q\downarrow})$	$c_5(\theta)$
$A_{P\downarrow Q\uparrow}^{R\downarrow S\uparrow} (h_{R\uparrow S\downarrow} + n_{R\uparrow S\downarrow})$	$c_5(\theta)$
$A_{P\downarrow Q\uparrow}^{R\downarrow S\uparrow} (n_{R\uparrow} h_{P\uparrow Q\downarrow} + n_{P\uparrow Q\downarrow} h_{R\uparrow})$	$c_6(\theta)$
$A_{P\downarrow Q\uparrow}^{R\downarrow S\uparrow} (n_{R\uparrow S\downarrow} h_{P\uparrow} + n_{P\uparrow} h_{R\uparrow S\downarrow})$	$c_6(\theta)$
$A_{P\downarrow Q\uparrow}^{R\downarrow S\uparrow} (n_{S\downarrow} h_{P\uparrow Q\downarrow} + n_{P\uparrow Q\downarrow} h_{S\downarrow})$	$c_6(\theta)$
$A_{P\downarrow Q\uparrow}^{R\downarrow S\uparrow} (n_{R\uparrow S\downarrow} h_{Q\downarrow} + n_{Q\downarrow} h_{R\uparrow S\downarrow})$	$c_6(\theta)$
$A_{P\downarrow Q\uparrow}^{R\downarrow S\uparrow} (n_{R\uparrow S\downarrow} h_{P\uparrow Q\downarrow} + n_{P\uparrow Q\downarrow} h_{R\uparrow S\downarrow})$	$c_7(\theta)$
$A_{P\downarrow Q\uparrow}^{R\downarrow S\uparrow} (n_{Q\downarrow R\uparrow} h_{P\uparrow S\downarrow} + n_{P\uparrow S\downarrow} h_{Q\downarrow R\uparrow})$	$c_8(\theta)$
$A_{P\downarrow Q\uparrow}^{R\downarrow S\uparrow} (h_{P\uparrow Q\downarrow R\uparrow S\downarrow} + n_{P\uparrow Q\downarrow R\uparrow S\downarrow})$	$c_8(\theta)$
$A_{P\uparrow Q\downarrow}^{R\downarrow S\uparrow}$	$\frac{\theta}{2\sqrt{3}}$
$A_{P\uparrow Q\downarrow}^{R\downarrow S\uparrow} (n_{R\uparrow} h_{Q\uparrow} + n_{Q\uparrow} h_{R\uparrow})$	$c_9(\theta)$
$A_{P\uparrow Q\downarrow}^{R\downarrow S\uparrow} (n_{S\downarrow} h_{P\downarrow} + n_{P\downarrow} h_{S\downarrow})$	$c_9(\theta)$
$A_{P\uparrow Q\downarrow}^{R\downarrow S\uparrow} (h_{R\uparrow S\downarrow} + n_{R\uparrow S\downarrow})$	$c_9(\theta)$
$A_{P\uparrow Q\downarrow}^{R\downarrow S\uparrow} (h_{P\downarrow Q\uparrow} + n_{P\downarrow Q\uparrow})$	$c_9(\theta)$
$A_{P\uparrow Q\downarrow}^{R\downarrow S\uparrow} (n_{R\uparrow S\downarrow} h_{Q\uparrow} + n_{Q\uparrow} h_{R\uparrow S\downarrow})$	$c_{10}(\theta)$
$A_{P\uparrow Q\downarrow}^{R\downarrow S\uparrow} (n_{R\uparrow} h_{P\downarrow Q\uparrow} + n_{P\downarrow Q\uparrow} h_{R\uparrow})$	$c_{10}(\theta)$
$A_{P\uparrow Q\downarrow}^{R\downarrow S\uparrow} (n_{R\uparrow S\downarrow} h_{P\downarrow} + n_{P\downarrow} h_{R\uparrow S\downarrow})$	$c_{10}(\theta)$
$A_{P\uparrow Q\downarrow}^{R\downarrow S\uparrow} (n_{S\downarrow} h_{P\downarrow Q\uparrow} + n_{P\downarrow Q\uparrow} h_{S\downarrow})$	$c_{10}(\theta)$
$A_{P\uparrow Q\downarrow}^{R\downarrow S\uparrow} (n_{R\uparrow S\downarrow} h_{P\downarrow Q\uparrow} + n_{P\downarrow Q\uparrow} h_{R\uparrow S\downarrow})$	$c_{11}(\theta)$
$A_{P\uparrow Q\downarrow}^{R\downarrow S\uparrow} (n_{Q\uparrow S\downarrow} h_{P\downarrow R\uparrow} + n_{P\downarrow R\uparrow} h_{Q\uparrow S\downarrow})$	$c_{12}(\theta)$
$A_{P\uparrow Q\downarrow}^{R\downarrow S\uparrow} (h_{P\downarrow Q\uparrow R\uparrow S\downarrow} + n_{P\downarrow Q\uparrow R\uparrow S\downarrow})$	$c_{12}(\theta)$
$A_{P\downarrow Q\uparrow}^{R\uparrow S\downarrow}$	$\frac{\theta}{2\sqrt{3}}$
$A_{P\downarrow Q\uparrow}^{R\uparrow S\downarrow} (n_{S\uparrow} h_{P\uparrow} + n_{P\uparrow} h_{S\uparrow})$	$c_9(\theta)$
$A_{P\downarrow Q\uparrow}^{R\uparrow S\downarrow} (n_{R\downarrow} h_{Q\downarrow} + n_{Q\downarrow} h_{R\downarrow})$	$c_9(\theta)$
$A_{P\downarrow Q\uparrow}^{R\uparrow S\downarrow} (h_{P\uparrow Q\downarrow} + n_{P\uparrow Q\downarrow})$	$c_9(\theta)$
$A_{P\downarrow Q\uparrow}^{R\uparrow S\downarrow} (h_{R\downarrow S\uparrow} + n_{R\downarrow S\uparrow})$	$c_9(\theta)$
$A_{P\downarrow Q\uparrow}^{R\uparrow S\downarrow} (n_{S\uparrow} h_{P\uparrow Q\downarrow} + n_{P\uparrow Q\downarrow} h_{S\uparrow})$	$c_{10}(\theta)$

Continued on next page.

TABLE S2: Continued from previous page

Basis element	Wei–Norman coefficient
$A_{P\downarrow Q\uparrow}^{R\uparrow S\downarrow} (n_{R\downarrow S\uparrow}h_{P\uparrow} + n_{P\uparrow}h_{R\downarrow S\uparrow})$	$c_{10}(\theta)$
$A_{P\downarrow Q\uparrow}^{R\uparrow S\downarrow} (n_{R\downarrow}h_{P\uparrow Q\downarrow} + n_{P\uparrow Q\downarrow}h_{R\downarrow})$	$c_{10}(\theta)$
$A_{P\downarrow Q\uparrow}^{R\uparrow S\downarrow} (n_{R\downarrow S\uparrow}h_{Q\downarrow} + n_{Q\downarrow}h_{R\downarrow S\uparrow})$	$c_{10}(\theta)$
$A_{P\downarrow Q\uparrow}^{R\uparrow S\downarrow} (n_{R\downarrow S\uparrow}h_{P\uparrow Q\downarrow} + n_{P\uparrow Q\downarrow}h_{R\downarrow S\uparrow})$	$c_{11}(\theta)$
$A_{P\downarrow Q\uparrow}^{R\uparrow S\downarrow} (n_{Q\downarrow S\uparrow}h_{P\uparrow R\downarrow} + n_{P\uparrow R\downarrow}h_{Q\downarrow S\uparrow})$	$c_{12}(\theta)$
$A_{P\downarrow Q\uparrow}^{R\uparrow S\downarrow} (h_{P\uparrow Q\downarrow R\downarrow S\uparrow} + n_{P\uparrow Q\downarrow R\downarrow S\uparrow})$	$c_{12}(\theta)$
$A_{Q\uparrow S\downarrow}^{Q\downarrow S\uparrow} (n_{R\uparrow}h_{P\uparrow} - n_{P\uparrow}h_{R\uparrow})$	$c_{13}(\theta)$
$A_{Q\uparrow S\downarrow}^{Q\downarrow S\uparrow} (n_{R\downarrow}h_{P\downarrow} - n_{P\downarrow}h_{R\downarrow})$	$-c_{13}(\theta)$
$A_{Q\uparrow S\downarrow}^{Q\downarrow S\uparrow} (n_{R\uparrow}h_{P\uparrow R\downarrow} - n_{P\uparrow R\downarrow}h_{R\uparrow})$	$c_{14}(\theta)$
$A_{Q\uparrow S\downarrow}^{Q\downarrow S\uparrow} (n_{R\downarrow}h_{P\downarrow R\uparrow} - n_{P\downarrow R\uparrow}h_{R\downarrow})$	$-c_{14}(\theta)$
$A_{Q\uparrow S\downarrow}^{Q\downarrow S\uparrow} (n_{P\downarrow R\uparrow}h_{P\uparrow} - n_{P\uparrow}h_{P\downarrow R\uparrow})$	$c_{14}(\theta)$
$A_{Q\uparrow S\downarrow}^{Q\downarrow S\uparrow} (n_{P\downarrow}h_{P\uparrow R\downarrow} - n_{P\uparrow R\downarrow}h_{P\downarrow})$	$c_{14}(\theta)$
$A_{Q\uparrow S\downarrow}^{Q\downarrow S\uparrow} (n_{P\downarrow R\uparrow}h_{P\uparrow R\downarrow} - n_{P\uparrow R\downarrow}h_{P\downarrow R\uparrow})$	$c_{15}(\theta)$
$A_{Q\uparrow S\downarrow}^{Q\downarrow S\uparrow} (n_{R\uparrow R\downarrow}h_{P\uparrow P\downarrow} - n_{P\uparrow P\downarrow}h_{R\uparrow R\downarrow})$	0
$A_{P\uparrow R\downarrow}^{P\downarrow R\uparrow} (n_{S\uparrow}h_{Q\uparrow} - n_{Q\uparrow}h_{S\uparrow})$	$c_{13}(\theta)$
$A_{P\uparrow R\downarrow}^{P\downarrow R\uparrow} (n_{S\downarrow}h_{Q\downarrow} - n_{Q\downarrow}h_{S\downarrow})$	$-c_{13}(\theta)$
$A_{P\uparrow R\downarrow}^{P\downarrow R\uparrow} (n_{Q\downarrow S\uparrow}h_{Q\uparrow} - n_{Q\uparrow}h_{Q\downarrow S\uparrow})$	$c_{14}(\theta)$
$A_{P\uparrow R\downarrow}^{P\downarrow R\uparrow} (n_{S\uparrow}h_{Q\uparrow S\downarrow} - n_{Q\uparrow S\downarrow}h_{S\uparrow})$	$c_{14}(\theta)$
$A_{P\uparrow R\downarrow}^{P\downarrow R\uparrow} (n_{S\downarrow}h_{Q\downarrow S\uparrow} - n_{Q\downarrow S\uparrow}h_{S\downarrow})$	$-c_{14}(\theta)$
$A_{P\uparrow R\downarrow}^{P\downarrow R\uparrow} (n_{Q\downarrow}h_{Q\uparrow S\downarrow} - n_{Q\uparrow S\downarrow}h_{Q\downarrow})$	$c_{14}(\theta)$
$A_{P\uparrow R\downarrow}^{P\downarrow R\uparrow} (n_{Q\downarrow S\uparrow}h_{Q\uparrow S\downarrow} - n_{Q\uparrow S\downarrow}h_{Q\downarrow S\uparrow})$	$c_{15}(\theta)$
$A_{P\uparrow R\downarrow}^{P\downarrow R\uparrow} (n_{S\uparrow S\downarrow}h_{Q\uparrow Q\downarrow} - n_{Q\uparrow Q\downarrow}h_{S\uparrow S\downarrow})$	0
$A_{Q\uparrow R\downarrow}^{Q\downarrow R\uparrow} (n_{S\uparrow}h_{P\uparrow} - n_{P\uparrow}h_{S\uparrow})$	$c_{16}(\theta)$
$A_{Q\uparrow R\downarrow}^{Q\downarrow R\uparrow} (n_{S\downarrow}h_{P\downarrow} - n_{P\downarrow}h_{S\downarrow})$	$-c_{16}(\theta)$
$A_{Q\uparrow R\downarrow}^{Q\downarrow R\uparrow} (n_{S\uparrow}h_{P\uparrow S\downarrow} - n_{P\uparrow S\downarrow}h_{S\uparrow})$	$c_{17}(\theta)$
$A_{Q\uparrow R\downarrow}^{Q\downarrow R\uparrow} (n_{P\downarrow S\uparrow}h_{P\uparrow} - n_{P\uparrow}h_{P\downarrow S\uparrow})$	$c_{17}(\theta)$
$A_{Q\uparrow R\downarrow}^{Q\downarrow R\uparrow} (n_{P\downarrow}h_{P\uparrow S\downarrow} - n_{P\uparrow S\downarrow}h_{P\downarrow})$	$c_{17}(\theta)$
$A_{Q\uparrow R\downarrow}^{Q\downarrow R\uparrow} (n_{S\downarrow}h_{P\downarrow S\uparrow} - n_{P\downarrow S\uparrow}h_{S\downarrow})$	$-c_{17}(\theta)$
$A_{Q\uparrow R\downarrow}^{Q\downarrow R\uparrow} (n_{P\downarrow S\uparrow}h_{P\uparrow S\downarrow} - n_{P\uparrow S\downarrow}h_{P\downarrow S\uparrow})$	$c_{18}(\theta)$
$A_{Q\uparrow R\downarrow}^{Q\downarrow R\uparrow} (n_{S\uparrow S\downarrow}h_{P\uparrow P\downarrow} - n_{P\uparrow P\downarrow}h_{S\uparrow S\downarrow})$	0
$A_{P\uparrow S\downarrow}^{P\downarrow S\uparrow} (n_{R\uparrow}h_{Q\uparrow} - n_{Q\uparrow}h_{R\uparrow})$	$c_{16}(\theta)$
$A_{P\uparrow S\downarrow}^{P\downarrow S\uparrow} (n_{R\downarrow}h_{Q\downarrow} - n_{Q\downarrow}h_{R\downarrow})$	$-c_{16}(\theta)$
$A_{P\uparrow S\downarrow}^{P\downarrow S\uparrow} (n_{Q\downarrow R\uparrow}h_{Q\uparrow} - n_{Q\uparrow}h_{Q\downarrow R\uparrow})$	$c_{17}(\theta)$

Continued on next page.

TABLE S2: Continued from previous page

Basis element	Wei–Norman coefficient
$A_{P\uparrow S\downarrow}^{P\downarrow S\uparrow} (n_{R\uparrow}h_{Q\uparrow R\downarrow} - n_{Q\uparrow R\downarrow}h_{R\uparrow})$	$c_{17}(\theta)$
$A_{P\uparrow S\downarrow}^{P\downarrow S\uparrow} (n_{R\downarrow}h_{Q\downarrow R\uparrow} - n_{Q\downarrow R\uparrow}h_{R\downarrow})$	$-c_{17}(\theta)$
$A_{P\uparrow S\downarrow}^{P\downarrow S\uparrow} (n_{Q\downarrow}h_{Q\uparrow R\downarrow} - n_{Q\uparrow R\downarrow}h_{Q\downarrow})$	$c_{17}(\theta)$
$A_{P\uparrow S\downarrow}^{P\downarrow S\uparrow} (n_{Q\downarrow R\uparrow}h_{Q\uparrow R\downarrow} - n_{Q\uparrow R\downarrow}h_{Q\downarrow R\uparrow})$	$c_{18}(\theta)$
$A_{P\uparrow S\downarrow}^{P\downarrow S\uparrow} (n_{R\uparrow R\downarrow}h_{Q\uparrow Q\downarrow} - n_{Q\uparrow Q\downarrow}h_{R\uparrow R\downarrow})$	0
<hr/>	
$A_{R\uparrow S\downarrow}^{R\downarrow S\uparrow} (h_{P\uparrow Q\downarrow} - n_{P\uparrow Q\downarrow})$	$c_{19}(\theta)$
$A_{R\uparrow S\downarrow}^{R\downarrow S\uparrow} (h_{P\downarrow Q\uparrow} - n_{P\downarrow Q\uparrow})$	$-c_{19}(\theta)$
$A_{R\uparrow S\downarrow}^{R\downarrow S\uparrow} (n_{Q\uparrow}h_{P\uparrow Q\downarrow} - n_{P\uparrow}h_{Q\uparrow})$	$c_{20}(\theta)$
$A_{R\uparrow S\downarrow}^{R\downarrow S\uparrow} (n_{P\downarrow}h_{P\uparrow Q\downarrow} - n_{P\uparrow}h_{P\downarrow Q\uparrow})$	$c_{20}(\theta)$
$A_{R\uparrow S\downarrow}^{R\downarrow S\uparrow} (n_{P\downarrow}h_{P\downarrow Q\uparrow} - n_{P\uparrow}h_{P\uparrow Q\downarrow})$	$c_{20}(\theta)$
$A_{R\uparrow S\downarrow}^{R\downarrow S\uparrow} (n_{Q\downarrow}h_{P\downarrow Q\uparrow} - n_{P\downarrow}h_{Q\downarrow})$	$-c_{20}(\theta)$
$A_{R\uparrow S\downarrow}^{R\downarrow S\uparrow} (n_{P\downarrow}h_{Q\uparrow}h_{P\uparrow Q\downarrow} - n_{P\uparrow}h_{Q\downarrow}h_{P\downarrow Q\uparrow})$	$c_{21}(\theta)$
$A_{R\uparrow S\downarrow}^{R\downarrow S\uparrow} (h_{P\uparrow P\downarrow Q\uparrow Q\downarrow} - n_{P\uparrow P\downarrow Q\uparrow Q\downarrow})$	0
<hr/>	
$A_{P\uparrow Q\downarrow}^{P\downarrow Q\uparrow} (h_{R\uparrow S\downarrow} - n_{R\uparrow S\downarrow})$	$c_{19}(\theta)$
$A_{P\uparrow Q\downarrow}^{P\downarrow Q\uparrow} (h_{R\downarrow S\uparrow} - n_{R\downarrow S\uparrow})$	$-c_{19}(\theta)$
$A_{P\uparrow Q\downarrow}^{P\downarrow Q\uparrow} (n_{S\uparrow}h_{R\uparrow S\downarrow} - n_{R\uparrow}h_{S\uparrow})$	$c_{20}(\theta)$
$A_{P\uparrow Q\downarrow}^{P\downarrow Q\uparrow} (n_{R\downarrow}h_{S\uparrow}h_{R\uparrow} - n_{R\uparrow}h_{S\uparrow}h_{R\downarrow})$	$c_{20}(\theta)$
$A_{P\uparrow Q\downarrow}^{P\downarrow Q\uparrow} (n_{R\downarrow}h_{R\uparrow S\downarrow} - n_{R\uparrow}h_{S\downarrow}h_{R\downarrow})$	$c_{20}(\theta)$
$A_{P\uparrow Q\downarrow}^{P\downarrow Q\uparrow} (n_{S\downarrow}h_{R\uparrow S\downarrow} - n_{R\uparrow}h_{S\downarrow})$	$-c_{20}(\theta)$
$A_{P\uparrow Q\downarrow}^{P\downarrow Q\uparrow} (n_{R\downarrow}h_{S\uparrow}h_{R\uparrow S\downarrow} - n_{R\uparrow}h_{S\downarrow}h_{R\downarrow})$	$c_{21}(\theta)$
$A_{P\uparrow Q\downarrow}^{P\downarrow Q\uparrow} (h_{R\uparrow R\downarrow S\uparrow S\downarrow} - n_{R\uparrow R\downarrow S\uparrow S\downarrow})$	0

^aThin partial horizontal rules separate basis elements that differ in the anti-Hermitian excitation part. Thick horizontal rules separate mutually commuting sets.

S6. CNOT-EFFICIENT QUANTUM CIRCUITS OF SYMMETRY-ADAPTED UNITARIES

In the Wei–Norman decompositions reported in the main text, there are ten types of generators besides simple spinorbital excitation operators. Examples from each category include $A_{P\uparrow Q\downarrow}^{R\uparrow S\downarrow} (h_{P\downarrow}h_{Q\uparrow} + n_{P\downarrow}h_{Q\uparrow})$, $A_{P\uparrow Q\downarrow}^{R\uparrow S\downarrow} (n_{Q\uparrow}h_{S\uparrow} + h_{Q\uparrow}n_{S\uparrow})$, $A_{P\uparrow Q\downarrow}^{R\uparrow S\downarrow} (n_{S\uparrow}h_{P\downarrow} + n_{P\downarrow}h_{S\uparrow})$, $A_{P\uparrow Q\downarrow}^{R\uparrow S\downarrow} (h_{P\downarrow}h_{Q\uparrow R\downarrow} + n_{P\downarrow}h_{Q\uparrow R\downarrow})$, $A_{P\uparrow Q\downarrow}^{R\uparrow S\downarrow} (h_{P\downarrow}h_{Q\uparrow}n_{R\downarrow} + n_{P\downarrow}h_{Q\uparrow}h_{R\downarrow})$, $A_{P\uparrow Q\downarrow}^{P\downarrow Q\uparrow} (h_{R\uparrow}h_{S\downarrow} - n_{R\uparrow}h_{S\downarrow})$, $A_{P\uparrow Q\downarrow}^{P\downarrow Q\uparrow} (n_{S\uparrow}h_{R\uparrow}h_{S\downarrow} - n_{R\uparrow}h_{S\downarrow})$, $A_{P\uparrow Q\downarrow}^{P\downarrow Q\uparrow} (h_{R\uparrow}h_{R\downarrow}h_{S\uparrow} - n_{R\uparrow}h_{R\downarrow}h_{S\uparrow})$, $A_{P\uparrow Q\downarrow}^{P\downarrow Q\uparrow} (h_{R\uparrow}h_{S\downarrow}h_{R\downarrow} - n_{R\uparrow}h_{S\downarrow}h_{R\downarrow})$, $A_{P\uparrow Q\downarrow}^{P\downarrow Q\uparrow} (h_{R\uparrow}h_{S\downarrow}h_{R\downarrow}h_{S\uparrow} - n_{R\uparrow}h_{S\downarrow}h_{R\downarrow}h_{S\uparrow})$, and $A_{Q\uparrow R\downarrow}^{Q\downarrow R\uparrow} (h_{P\uparrow}h_{S\uparrow} - n_{P\uparrow}h_{S\uparrow})$. In Figs. 7 and 8 of the main text, we showed the CNOT-efficient quantum circuits implementing the unitaries generated by $A_{P\uparrow Q\downarrow}^{R\uparrow S\downarrow} (h_{P\downarrow}h_{Q\uparrow} + n_{P\downarrow}h_{Q\uparrow})$ and $A_{P\uparrow Q\downarrow}^{P\downarrow Q\uparrow} (h_{R\uparrow}h_{S\downarrow} - n_{R\uparrow}h_{S\downarrow})$. Below, we provide the corresponding circuits for the unitaries generated by the remaining operators.

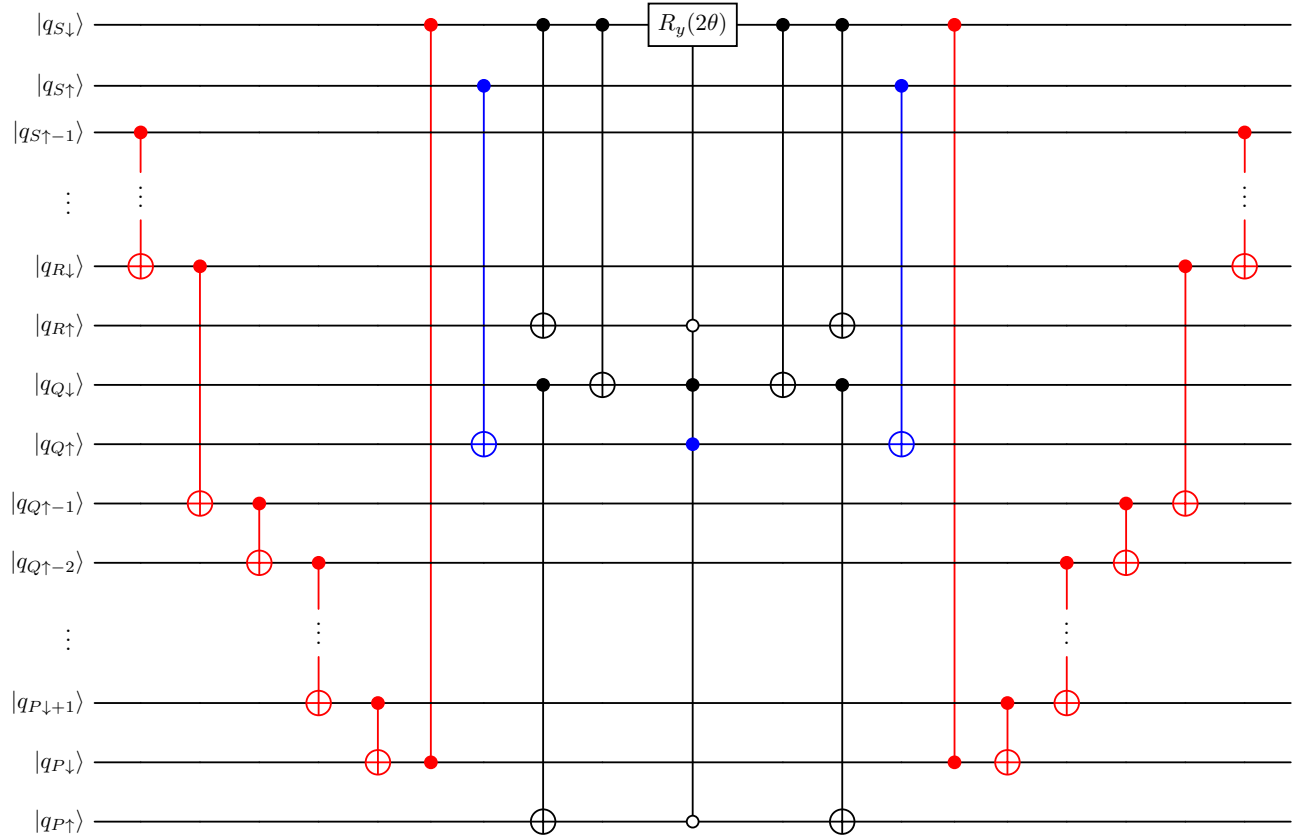


FIG. S6. Fermionic excitation-based quantum circuit implementing $\exp\left[\theta A_{P\uparrow Q\downarrow}^{R\uparrow S\downarrow}(n_{Q\uparrow}h_{S\uparrow} + h_{Q\uparrow}n_{S\uparrow})\right]$.

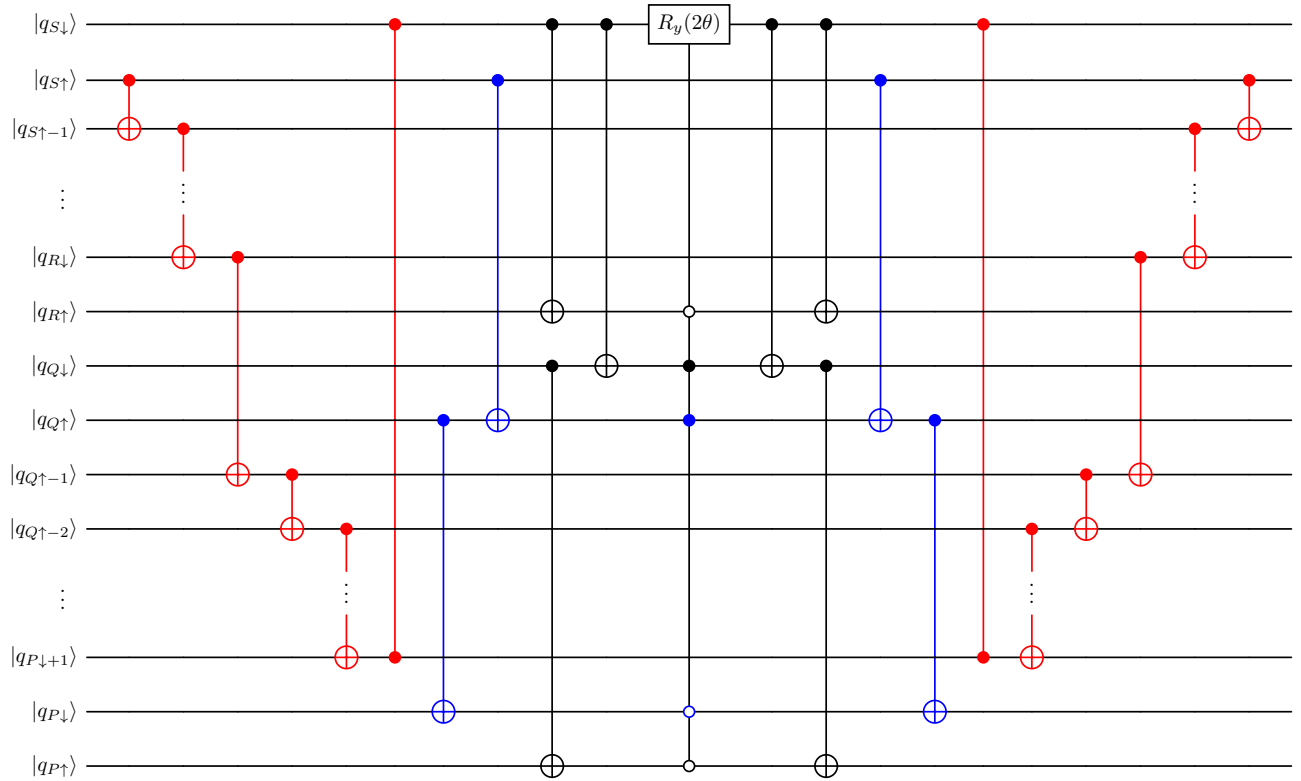


FIG. S7. Fermionic excitation-based quantum circuit implementing $\exp\left[\theta A_{P\uparrow Q\downarrow}^{R\uparrow S\downarrow} (h_{P\downarrow Q\uparrow} n_{S\uparrow} + n_{P\downarrow Q\uparrow} h_{S\uparrow})\right]$.

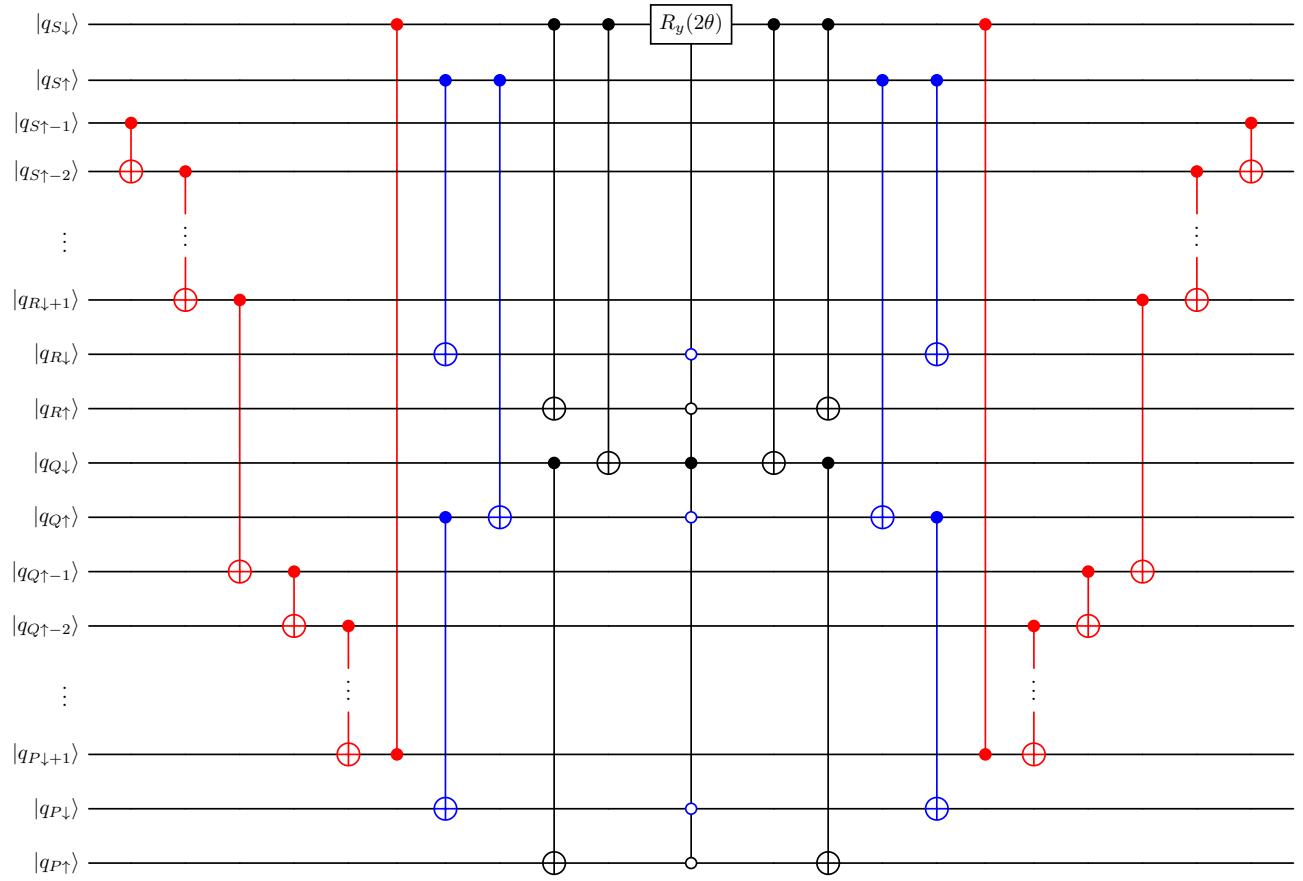


FIG. S8. Fermionic excitation-based quantum circuit implementing $\exp\left[\theta A_{P\uparrow Q\downarrow}^{R\uparrow S\downarrow}(h_{P\downarrow Q\uparrow R\downarrow S\uparrow} + n_{P\downarrow Q\uparrow R\downarrow S\uparrow})\right]$.

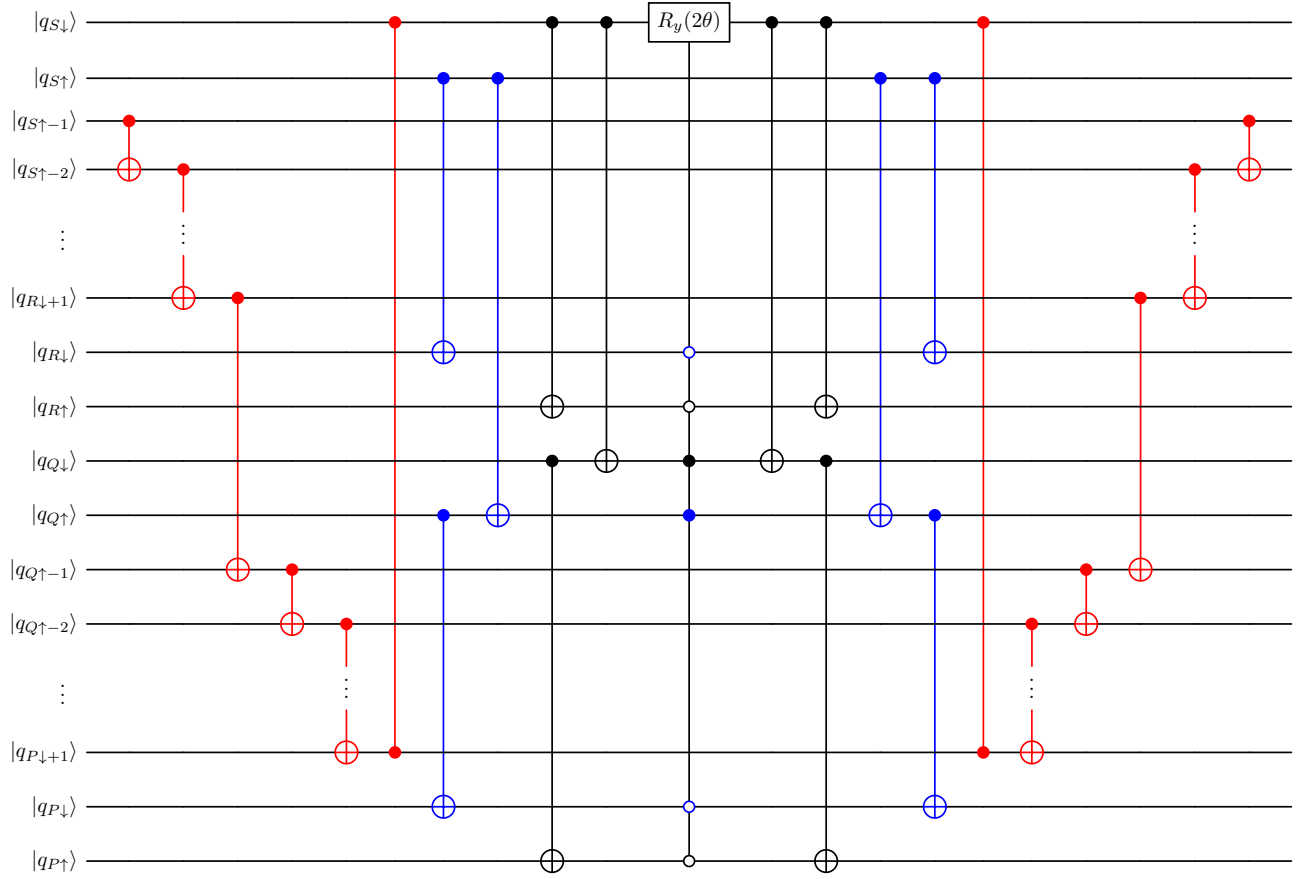


FIG. S9. Fermionic excitation-based quantum circuit implementing $\exp\left[\theta A_{P\uparrow Q\downarrow}^{R\uparrow S\downarrow}(h_{P\downarrow Q\uparrow}n_{R\downarrow S\uparrow} + n_{P\downarrow Q\uparrow}h_{R\downarrow S\uparrow})\right]$.

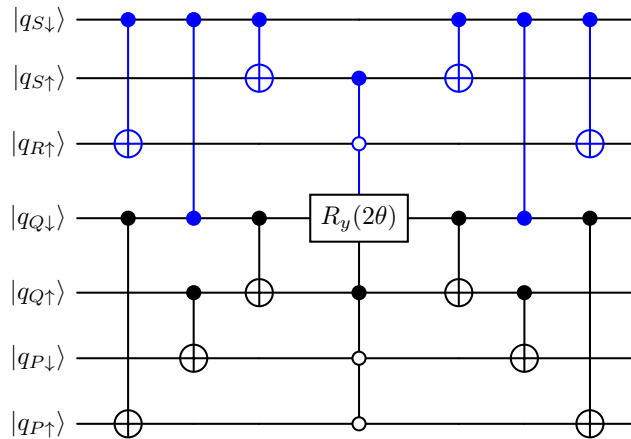


FIG. S10. Fermionic excitation-based quantum circuit implementing $\exp\left[\theta A_{P\uparrow Q\downarrow}^{P\downarrow Q\uparrow}(h_{R\uparrow S\downarrow}n_{S\uparrow} - n_{R\uparrow S\downarrow}h_{S\uparrow})\right]$.

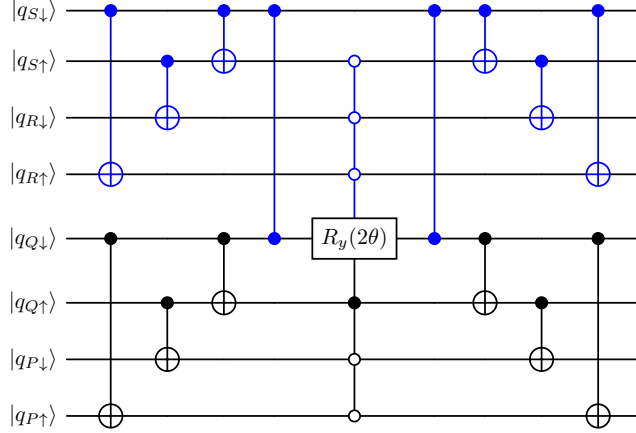


FIG. S11. Fermionic excitation-based quantum circuit implementing $\exp\left[\theta A_{P\uparrow Q\downarrow}^{P\downarrow Q\uparrow}(h_{R\uparrow R\downarrow S\uparrow S\downarrow} - n_{R\uparrow R\downarrow S\uparrow S\downarrow})\right]$.

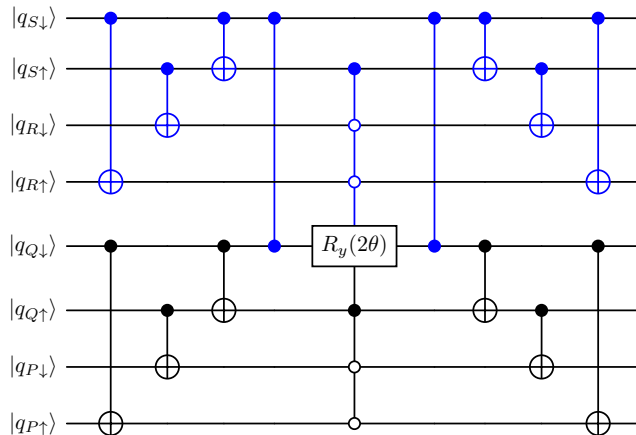


FIG. S12. Fermionic excitation-based quantum circuit implementing $\exp\left[\theta A_{P\uparrow Q\downarrow}^{P\downarrow Q\uparrow}(h_{R\uparrow S\downarrow n_{R\downarrow S\uparrow} - n_{R\uparrow S\downarrow} h_{R\downarrow S\uparrow})\right]$.

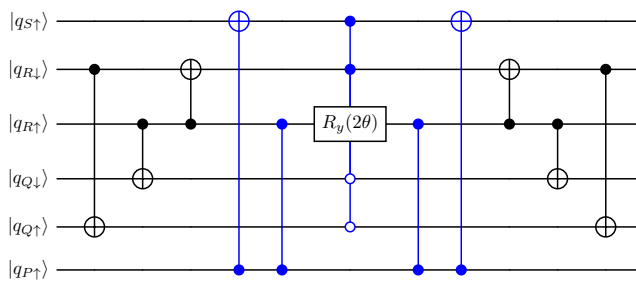


FIG. S13. Fermionic excitation-based quantum circuit implementing $\exp\left[\theta A_{Q\uparrow R\downarrow}^{Q\downarrow R\uparrow}(h_{P\uparrow n_{S\uparrow} - n_{P\uparrow} h_{S\uparrow})\right]$.

S7. NUCLEAR COORDINATES OF THE H₆ SYSTEM

TABLE S3. Nuclear coordinates (in Å) defining the D_{2h} -symmetric distorted hexagonal H₆ structure used in the numerical simulations reported in the main text.

atom	<i>x</i>	<i>y</i>	<i>z</i>
H1	3	0	0
H2	-3	0	0
H3	2	$\sqrt{3}$	0
H4	2	$-\sqrt{3}$	0
H5	-2	$\sqrt{3}$	0
H6	-2	$-\sqrt{3}$	0

S8. ALTERNATIVE EXACT PRODUCT FORMULAS

As mentioned in the main text, since the spinorbital operators that define spin-adapted unitaries generate finite Lie algebras, it might be possible to construct exact, finite product formulas reminiscent of finite-order Trotter–Suzuki decompositions. We tested this numerically in the case of the simplest, yet nontrivial, spin-adapted unitary, $\exp\left[\theta(A_{P\uparrow P\downarrow}^{Q\uparrow R\downarrow} - A_{P\uparrow P\downarrow}^{Q\downarrow R\uparrow})/\sqrt{2}\right]$. For the sake of brevity, we set $A \equiv A_{P\uparrow P\downarrow}^{Q\uparrow R\downarrow}$ and $B \equiv A_{P\uparrow P\downarrow}^{Q\downarrow R\uparrow}$. Based on our numerical explorations, the minimum number of exponentials required is six, leading to the product formula

$$e^{\frac{\theta}{\sqrt{2}}(A-B)} = e^{\alpha_1(\theta)A} e^{\alpha_2(\theta)B} e^{\alpha_3(\theta)A} e^{\alpha_4(\theta)B} e^{\alpha_5(\theta)A} e^{\alpha_6(\theta)B}, \quad (\text{S11})$$

with the optimum values of the θ -dependent parameters given in Fig. S14.

The computational protocol we adopted is as follows. We constructed the matrix representation of both the target unitary and the product ansatz in a minimal Fock space of 6 spinorbitals. For each $\theta \in [0, 10]$, sampled on 2001 uniformly spaced points, we minimized the Frobenius norm of the difference between these two matrices using the least-squares optimizer of SciPy. We employed tight convergence criteria ($\text{xtol} = \text{ftol} = \text{gtol} = 10^{-12}$) and set the maximum number of function evaluations to $\text{max_nfev} = 3000$. To increase confidence that the global minimum was obtained, for every value of θ we performed 20 restarts with random initial parameter values. The maximum residual Frobenius error over the grid was $\approx 10^{-16}$.

In contrast to the Wei–Norman decomposition, the parameters entering Eq. (S11) are not uniquely defined. Nevertheless, the algebraic structure does impose constraints on the parameters. For

example, we find that

$$\alpha_1(\theta) + \alpha_3(\theta) + \alpha_5(\theta) = \frac{\theta}{\sqrt{2}} \quad (\text{S12})$$

and

$$\alpha_2(\theta) + \alpha_4(\theta) + \alpha_6(\theta) = \frac{\theta}{\sqrt{2}}. \quad (\text{S13})$$

A major issue in the practical utility of such decompositions is that the parameters are highly oscillatory functions of θ , rendering them more sensitive to device noise and complicating the computation of derivatives.

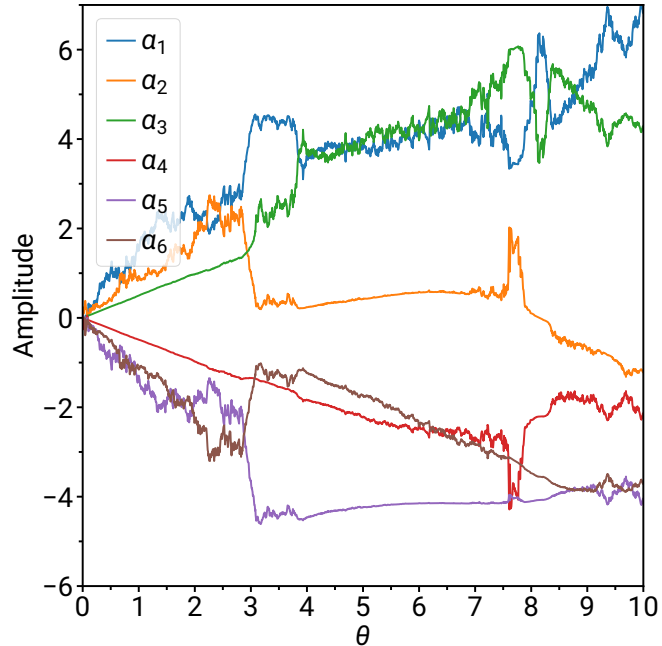


FIG. S14. Numerical values of the θ -dependent parameters defining the Trotter–Suzuki-like decomposition of Eq. (S11).